

# Self-consistent solution of Kohn-Sham equations for infinitely extended systems with inhomogeneous electron gas

D. V. Posvyanskii and A. Ya. Shul'man

Kotel'nikov Institute of Radio Engineering and Electronics of RAS,  
Moscow, 125009 Russia

## Abstract

The density functional approach in the Kohn-Sham approximation is widely used to study properties of many-electron systems. Due to the nonlinearity of the Kohn-Sham equations, the general self-consistence searching method involves iterations with alternate solving of the Poisson and Schrödinger equations. One of problems of such an approach is that the charge distribution renewed by means of the Schrödinger equation solution does not conform to boundary conditions of Poisson equation for Coulomb potential. The resulting instability or even divergence of iterations manifests itself most appreciably in the case of infinitely extended systems. The published attempts to deal with this problem are reduced in fact to abandoning the original iterative method and replacing it with some approximate calculation scheme, which is usually semi-empirical and does not permit to evaluate the extent of deviation from the exact solution. In this work, we realize the iterative scheme of solving the Kohn-Sham equations for extended systems with inhomogeneous electron gas, which is based on eliminating the long-range character of Coulomb interaction as the cause of tight coupling between charge distribution and boundary conditions. The suggested algorithm is employed to calculate energy spectrum, self-consistent potential, and electrostatic capacitance of the semi-infinite degenerate electron gas bounded by infinitely high barrier, as well as the work function and surface energy of simple metals in the model with homogeneous distribution of positive background. The difference between self-consistent Hartree solutions and those taking into account the exchange-correlation interaction is analyzed. The comparison with results previously published in the literature is carried out. The case study of the metal-semiconductor tunnel contact shows this method being applied to an infinitely extended system where the steady-state current can flow.

PACS:71.15.-m, 71.15.Mb, 65.40.gh, 85.30.Mn

## 1 Introduction

In the density functional approach, the set of equations describing the inhomogeneous electron gas in the Kohn-Sham approximation should be satisfied by the self-consistent distribution of electron density  $N(\mathbf{r})$  and Coulomb potential  $U(\mathbf{r})$  [1]. Due to the essential nonlinearity of these equations, the only general method of self-consistent solution involves iterations using

alternately the Poisson equation for potential and the set of Schrödinger equations for single-particle wave functions in the effective potential  $U_{\text{eff}}(\mathbf{r}) = U(\mathbf{r}) + U_{\text{xc}}(\mathbf{r})$ , where  $U_{\text{xc}}$  is the exchange-correlation potential in the local density approximation. A well-known problem of such an approach lies in the necessity of taking into account the boundary conditions of the Poisson equation, which impose certain requirements in terms of integral relations on the charge distribution in the right-hand side of this equation [2]. From the physical point of view, these integral relations specify, for example, the total charge of the electron system, if the boundary conditions are imposed on the electric field, or the total dipole moment of the system, if the values of potential on the boundaries of an infinite region are fixed.

However, until the self-consistency is reached, the distribution of electron density found by means of the Schrödinger equation at each step of iteration process turns out, as a rule, to be incompatible with the Poisson boundary conditions specified. Consequently, as shown in [2], in the case of infinitely extended systems it is either not possible to build the next step solution at all, or the iteration process lacks convergence as reported, for example, in [3, 4]. In such a situation, some authors resort to replacing the process of solving the Poisson equation with some kind of variation scheme relative to numerical parameters that specify the functional form chosen to approximate the potential or charge distribution. This is discussed in more detail in subsections 3.1 and 4.1.

To manage this difficulty there are several artificial techniques suggested, all of them changing the parameters of the system in question, for example, the compensating background charge density [5]. However, the existence and uniqueness of the solution of self-consistent field equations follows from their being obtained as Euler-Lagrange equations for a variational problem of minimizing the total energy of non-degenerate ground state (see, for example, [1]). In such a case the single-particle orbital wave functions and Coulomb potential are varied at fixed boundary conditions, while the parameters of the system remain constant. For varying the system parameters over the iteration process one needs a proof of existence and uniqueness of solution, which is now absent.

Another approach suggested in [4, 6] finds the electrostatic potential  $U(\mathbf{r})$  by means of a linear integral equation of the second kind, to which the Poisson equation is artificially reduced. In so doing, the necessity of special measures to maintain compatibility of the Poisson boundary conditions with charge distribution obtained at each iteration is allegedly eliminated (see [6], Appendix). However it is clear that the exact solution of integral equation, which is equivalent to the original differential one, does not exist either, if some of the compatibility conditions fail to hold. Apparently for this reason, the said method, even if successful, was complemented at each iteration by some unclear renormalization of electron density obtained by means of the Schrödinger equation to fulfil the neutrality condition before solving the Poisson equation [4]. One more drawback of this approach appears to be, in fact, the conservation of screening term in the region without electrons but with nonzero potential, as it is the case in the surface problems.

In this work we realize the iteration algorithm suggested earlier and described in [2], which is applicable to solving the Kohn-Sham equations for the equilibrium inhomogeneous electron gas and satisfies the boundary conditions for the Poisson equation at any shape of electron distribution induced by the effective potential of the previous approximation (section 2). The algorithm peculiarities caused by discontinuity of quasiclassical expression for the induced electron density with exchange-correlation potential taken into account are pointed out (section 2.2). The convergence of the algorithm is demonstrated by example of self-consistent calculations in a model with homogeneous compensating background while studying such problems

as: 1) self-induced bound states near the surface of barrier-bounded electron gas (section 3.1), 2) parallel-plate capacitor with real distribution of screening charge accounting for Friedel oscillations of electron density (section 3.2), 3) work function and surface energy of simple metals (section 4). The example of a metal-semiconductor tunneling contact with Schottky barrier is used to demonstrate the method's applicability to the systems where the current flow is possible (section 5). Some of the results were preliminarily presented in [7] and reported to the Russian conferences on semiconductor physics in 2001 - 2007.

## 2 The base equations and iteration algorithm

### 2.1 General formulation

In the Kohn-Sham approximation, the gas of interacting electrons at temperature  $T = 0$  is described by the set of equations for single-particle wave functions  $\Psi_\varepsilon$

$$\frac{1}{2}\nabla^2\Psi_\varepsilon(\mathbf{r}) + (\varepsilon - U_{\text{eff}}(\mathbf{r}))\Psi_\varepsilon(\mathbf{r}) = 0 \quad (2.1)$$

with the effective potential

$$U_{\text{eff}}(\mathbf{r}) = U(\mathbf{r}) + U_{\text{xc}}(\mathbf{r}). \quad (2.2)$$

Here  $\varepsilon$  is the energy eigenvalue of a single-particle state, and  $U$  is Coulomb potential energy of the electron described by the Poisson equation

$$\nabla^2 U = 4\pi(N_+(\mathbf{r}) - N(\mathbf{r})), \quad (2.3)$$

where  $N_+(\mathbf{r})$  is positive charge density,  $N(\mathbf{r})$  is electron density. Everywhere, unless otherwise specified, the atomic units  $|e| = m = \hbar = 1$  are used based on charge  $e$  and mass  $m$  of the free electron, when the unit of distance is Bohr radius  $a_B$ , and the unit of energy is Hartree  $Ha = e^2/a_B$ .

The exchange-correlation potential in equation (2.2) is taken in the local approximation of density functional

$$U_{\text{xc}}(\mathbf{r}) = \left. \frac{d[N\varepsilon_{\text{xc}}(N)]}{dN} \right|_{N=N(\mathbf{r})}, \quad (2.4)$$

where  $\varepsilon_{\text{xc}} = \varepsilon_x + \varepsilon_c$  is the sum of exchange and correlation energy per particle.

The electron density is expressed through wave functions as

$$N(\mathbf{r}) = 2 \int_{\varepsilon \leq \varepsilon_F} \mathfrak{D}\{\varepsilon\} |\Psi_\varepsilon(\mathbf{r})|^2, \quad (2.5)$$

where factor 2 takes into account the spin degeneracy of single-particle states, and the integration on differential spectral measure  $\mathfrak{D}\{\varepsilon\}$  of Hamiltonian  $\hat{H} = -\frac{1}{2}\nabla^2 + U_{\text{eff}}(\mathbf{r})$  is made over all occupied states with energy  $\varepsilon$  not exceeding the Fermi energy  $\varepsilon_F$ .

As pointed out in the Introduction, the boundary conditions for the Poisson equation impose certain requirements on the spatial distribution of electron density, and the result of integration in Eq. (2.5) does not necessarily comply with them until the self-consistency is reached. However, if we conceive of the total electron density as the sum

$$N(\mathbf{r}) = N_{\text{ind}}(U(\mathbf{r})) + N_{\text{qu}}(\mathbf{r}), \quad (2.6)$$

where the induced density  $N_{\text{ind}}$  depends explicitly on the unknown potential, the incompatibility problem of boundary conditions with the right-hand side of Poisson equation does not arise because the long-range Coulomb interaction is replaced with the screened interaction of finite range. In the Kohn-Sham theory, the electron density and effective potential can be coupled with an approximate local relation similar to that used for the classical ideal equilibrium Fermi gas

$$N_{\text{ind}}(\mathbf{r}) = \frac{2^{3/2}}{3\pi^2} (\varepsilon_{\text{F}} - U_{\text{eff}}(\mathbf{r}))^{3/2}. \quad (2.7)$$

Formula (2.7) can be obtained from the solutions of Schrödinger equation (2.1) for wave functions of continuous spectrum in quasiclassical approximation by substituting them into Eq. (2.5) and averaging the resulting electron density over a scale larger than the Fermi wavelength  $\lambda_{\text{F}}$ . The function  $N_{\text{qu}}(\mathbf{r})$  with  $N_{\text{ind}}(\mathbf{r})$  of Eq. (2.7) is a quantum correction to the quasiclassical electron distribution. Note that the representation of total density as in Eq. (2.6) is always exact regardless of using the approximate formula (2.7) for  $N_{\text{ind}}(\mathbf{r})$ .

In expression (2.2),  $U_{\text{xc}} = U_{\text{x}} + U_{\text{c}}$ . The exchange potential for electron gas in the local approximation is given by the well-known expression

$$U_{\text{x}}(\mathbf{r}) = - \left( \frac{3}{\pi} \right)^{1/3} N^{1/3}(\mathbf{r}) = - \left( \frac{3}{2\pi} \right)^{2/3} \frac{1}{r_{\text{s}}(\mathbf{r})}. \quad (2.8)$$

The correlation potential, according to Eq. (2.4), is defined through the correlation energy per particle  $\varepsilon_{\text{c}}$ . We assume the latter as

$$\varepsilon_{\text{c}} = - \frac{0.44}{r_{\text{s}} + 11.5}. \quad (2.9)$$

Here  $r_{\text{s}}$  is the local Wigner-Seitz radius defined as

$$4\pi r_{\text{s}}^3(\mathbf{r})/3 = N^{-1}(\mathbf{r}). \quad (2.10)$$

For the following analysis it is convenient to introduce  $R_{\text{s}} = r_{\text{s}}(\infty)$  as the value of this parameter at infinity, where we always take the local neutrality condition  $\lim_{|\mathbf{r}| \rightarrow \infty} (N - N_{+}) \rightarrow 0$  to be fulfilled.

Having calculated the derivative (2.4) with correlation energy given by Eq. (2.9), one can write the correlation potential as

$$U_{\text{c}}(\mathbf{r}) = - \frac{22}{75} \frac{8r_{\text{s}}(\mathbf{r}) + 69}{[2r_{\text{s}}(\mathbf{r}) + 23]^2}. \quad (2.11)$$

The formula (2.9) for correlation energy is a well-known Wigner expression with a different parameter 11.5 instead of 7.8 in denominator. The reasons for using the modified Wigner formula will be discussed in more detail elsewhere. Here we only note that such a choice of  $\varepsilon_{\text{c}}$ , on the one hand, describes better the  $R_{\text{s}}$  dependence of cohesive energy of simple metals represented in Table 8 of the book [8]. On the other hand, the value  $R_{\text{s}} = 5.63$  accepted in the literature for Cs turns out less than the critical one  $R_{\text{s}c} = 5.64$ , which characterizes the stability of homogeneous electron gas in the jellium model with respect to spatially inhomogeneous perturbations. The impossibility to use the formula (2.7) for induced charge in the case of  $R_{\text{s}} \geq R_{\text{s}c}$  would make the suggested algorithm inapplicable, so the choice of correlation energy in the form (2.9) provides the existence of cesium metal in the framework of calculation technique

under development. There are also other expressions suggested in the literature for correlation energy in the local density approximation LDA (see, for example, discussion in [1, 5]), but for the purposes of this work aimed at demonstrating in detail the application of the new algorithm to a number of classical problems, the specific form of correlation potential is not so important, because the relevant modifications to the expression for  $U_c$  lead to only quantitative changes in calculation results, and do not create fundamental difficulties for realization of iteration scheme suggested.

The separation of induced charge brings the Poisson equation (2.3) to the form

$$\nabla^2 U + 4\pi N_{\text{ind}}(U) = 4\pi(N_+(\mathbf{r}) - N_{\text{qu}}(\mathbf{r})). \quad (2.12)$$

The quantum correction to electron density  $N_{\text{qu}}(\mathbf{r})$  introduced here by means of Eqs. (2.5)-(2.7) is defined as

$$N_{\text{qu}}(\mathbf{r}) = 2 \int_{\varepsilon \leq \varepsilon_F} \mathfrak{D}\{\varepsilon\} |\Psi_\varepsilon(\mathbf{r})|^2 - N_{\text{ind}}(\mathbf{r}). \quad (2.13)$$

The algorithm of consecutive steps  $i = 0, 1, 2, \dots$  for iterative solving of equations (2.1) - (2.5) with equation (2.3) changed to (2.12) can be now formulated as follows:

1. Neglect the small-scale quantum variations of electron density

$$N_{\text{qu}}^0 = 0; \quad (2.14)$$

2. Solve the nonlinear Poisson equation with a known right-hand side

$$\nabla^2 U^i(\mathbf{r}) + 4\pi N_{\text{ind}}(U^i, N_{\text{qu}}^i) = 4\pi(N_+(\mathbf{r}) - N_{\text{qu}}^i(\mathbf{r})); \quad (2.15)$$

3. Find the total electron density self-consistent with  $U$ , and effective potential

$$N_s^i(\mathbf{r}) = N_{\text{ind}}^i(\mathbf{r}) + N_{\text{qu}}^i(\mathbf{r}); \quad U_{\text{eff}}^i(\mathbf{r}) = U^i(\mathbf{r}) + U_{\text{xc}}(N_s^i(\mathbf{r})); \quad (2.16)$$

4. Find the eigenfunctions of the single-particle Kohn-Sham Hamiltonian

$$\frac{1}{2} \nabla^2 \Psi_\varepsilon^i(\mathbf{r}) + (\varepsilon - U_{\text{eff}}^i(\mathbf{r})) \Psi_\varepsilon^i(\mathbf{r}) = 0; \quad (2.17)$$

5. Find anew the total electron density, using the eigenvalues and eigenfunctions obtained

$$N^i(\mathbf{r}) = 2 \int_{\varepsilon \leq \varepsilon_F} \mathfrak{D}\{\varepsilon\} |\Psi_\varepsilon^i(\mathbf{r})|^2; \quad (2.18)$$

6. Calculate the quantum correction for the next iteration step by means of the new total electron density

$$N_{\text{qu}}^{i+1}(\mathbf{r}) = N^i(\mathbf{r}) - N_{\text{ind}}(U_{\text{eff}}^i(\mathbf{r})); \quad (2.19)$$

7. Return to solving the Poisson equation with the new right-hand side.

Index  $i$  here denotes the iteration number. It is of importance that the Coulomb potential  $U^i(\mathbf{r})$  and the induced electron density  $N_{\text{ind}}^i(\mathbf{r})$  are found self-consistently at a fixed quantum density  $N_{\text{qu}}^i(\mathbf{r})$  in the process of solving the Poisson equation (2.15).

The convergence criterion for iteration process is the value of  $\delta$ , which limits the maximal deviation of the electron density  $N_s^i(\mathbf{r})$  obtained after solving the Poisson equation and self-consistent with the potential  $U^i(\mathbf{r})$ , from the density  $N^i(\mathbf{r})$  found by means of the Schrödinger equation,

$$\max_{\mathbf{r}} |N_s^i(\mathbf{r}) - N^i(\mathbf{r})| / N(\infty) \leq \delta. \quad (2.20)$$

It is assumed here that electron density at infinity is determined by the local neutrality condition and does not change through the iteration process.

In the course of solving the self-consistent Poisson equation (2.15), the induced density

$$N_{\text{ind}}^i = N_{\text{ind}}(U^i, N_{\text{qu}}^i)$$

should be calculated as an implicit function of unknown potential  $U^i$  at a known quantum correction  $N_{\text{qu}}^i$  according to formulae (2.2) and (2.7). It is implicit because the exchange-correlation potential in Eq. (2.7) depends on the total electron density  $N_{\text{ind}}^i + N_{\text{qu}}^i$ .

One should note that representing the induced charge as Eq. (2.7) requires the condition

$$\frac{dN_{\text{ind}}}{dU} < 0. \quad (2.21)$$

to be fulfilled.

Otherwise, the square of the linear screening length in the equation (2.15) linearized for  $U$  turns negative, and the response to small spatial perturbations of electron density is no more localized due to oscillating behavior of solutions of the self-consistent Poisson equation. The inequality (2.21) is generally violated in the regions where electron density is small and, accordingly, the relative role of exchange-correlation potential increases. In such regions of instability, the induced electron density cannot be represented with Eq. (2.7), so we take  $N_{\text{ind}}^i(\mathbf{r}) \equiv 0$ . This situation occurs, for example, near the surface of electron systems at the distribution tails where the electron density is close to zero.

To conclude this section, there are some remarks on terminology used further on. The result of self-consistent calculation by means of the complete set of equations (2.14)-(2.19) with expression (2.7) for the induced electron density, exchange potential as (2.8) and correlation potential (2.11) is called the exact or the self-consistent solution. Solving the same set of equations, but ignoring  $U_{\text{xc}}$ , one obtains the self-consistent solution in the Hartree approximation. The self-consistent solution of the Poisson equation (2.12) with the induced density (2.7), ignoring  $U_{\text{xc}}$ , and at  $N_{\text{qu}} = 0$  is the Thomas-Fermi approximation. If the exchange potential  $U_x$  is taken into account in the latter scheme, it becomes the Thomas-Fermi-Dirac approximation. Using the total effective potential in the local density approximation with the induced charge formula (2.7) is sometimes called the Thomas-Fermi-Dirac-Gombas approximation (see, for example, [9], Sec. 11).

## 2.2 Peculiarities of the algorithm application

The calculation technique using the induced electron density is clarified more specifically in further sections, where the suggested iteration algorithm is realized in calculating the quantum correction to the capacitance of barrier structures and in finding the work function and surface

energy of simple metals in the model with homogeneous positive background. At the same time, the homogeneity of background allows to get still further in the analytical transformation of the general equations. Let us consider the semiinfinite electron gas assuming that the ion charge forms a homogeneous positive background of density  $N_+$  given by

$$N_+(z) = \begin{cases} N_+, & z \geq z_+, \\ 0, & z < z_+. \end{cases} \quad (2.22)$$

In this model, the effective potential in the Schrödinger equation (2.17) depends solely on the coordinate  $z$ . Such system can represent, for example, a metal surface with self-consistent barrier or a semiconductor structure bounded by a potential barrier.

The expression for induced charge in the form (2.7) is asymptotically correct (with respect to quasiclassicality parameter, which is always small in the systems in question at  $z \rightarrow \infty$ ) in describing the self-consistent reaction of electrons to the change in the long-wave part of Coulomb potential, which is what is necessary to eliminate the infinite range of direct Coulomb interaction of electrons. However, as noted before, it fails in the regions of small electron density where the condition (2.21) does not hold. In view of the above, the self-consistent Poisson equation can be written as

$$\begin{aligned} \frac{d^2 u^i}{d\zeta^2} + c_n n_{\text{ind}}(u^i, n_{\text{qu}}^i) &= c_n (\theta(\zeta - \zeta_+) - n_{\text{qu}}^i(\zeta)), & \zeta > \zeta_c^i \\ \frac{d^2 u^i}{d\zeta^2} &= c_n (\theta(\zeta - \zeta_+) - n^i(\zeta)), & \zeta \leq \zeta_c^i \end{aligned} \quad (2.23)$$

where  $c_n = (8/3\pi)(4/9\pi)^{1/3} R_s$ , and  $\theta(\zeta)$  is the Heavyside theta function. We introduced the dimensionless variables  $\zeta = k_F z$ ,  $\zeta_+ = k_F z_+$ ,  $n(\zeta) = N(z)/N_+$ ,  $u(\zeta) = U(z)/\varepsilon_F^0$ , where  $k_F = (3\pi^2 N_+)^{1/3}$ ,  $\varepsilon_F^0 = k_F^2/2$ . The boundary conditions must force the electric field  $du/d\zeta$  to be zero at infinity, to ensure the potential finiteness,  $u(\infty) = \text{const}$ , and local neutrality of the electron gas,  $n(\infty) = 1$ .

Eq. (2.23) assumes the existence of a single critical point  $\zeta_c$  that separates the region with the induced density  $n_{\text{ind}}$  expressed as (2.7), from the region, where such expression is invalid according to criterion (2.21). When calculating the systems that meet the condition  $R_s < R_{\text{sc}}$ , it is always possible to introduce  $n_{\text{ind}}$  in the region  $\zeta_c^i < \zeta < \infty$ . The density  $n_{\text{qu}}^i$  turns out definite at the same region. Actually the problem is always solved on the finite interval of real axis,  $0 \leq \zeta \leq \zeta_{\text{max}}$ . The value  $\zeta_+ \geq 0$  denotes the possible shift of the positive background starting point from zero. Values  $\zeta_+$  and  $\zeta_{\text{max}}$  are assumed to be taken so large that the transfer of boundary conditions to the points  $\zeta = 0$  and  $\zeta_{\text{max}}$  from  $\zeta = -\infty$  and  $\zeta = \infty$  does not affect the result within the chosen accuracy. This condition is easily checked by calculations at several consecutively increasing values of  $\zeta_+$  and  $\zeta_{\text{max}}$ .

At the point  $\zeta_c$  the right-hand and left-hand solutions are matched together so that potential  $u$  is continuous along with its first derivative. The critical point  $\zeta_c$  is defined as the point where inequality(2.21) reverses its sign, that is, the derivative  $dn_{\text{ind}}/du$  turns positive. As long as with reversing sign the derivative of multivalued implicit function  $n_{\text{ind}}(u)$  passes through infinity, it is more convenient, in the manner of the density functional approach, to analyze the inverse single-valued function  $u(n_{\text{ind}})$ , whose derivative reverses its sign, passing through zero. This function can be found from formula (2.7) and in the dimensionless variables introduced has the form

$$u(n_{\text{ind}}) = \mu - n_{\text{ind}}^{2/3} - u_{\text{xc}}(n_{\text{ind}} + n_{\text{qu}}), \quad (2.24)$$

where  $u_{xc} = U_{xc}/\varepsilon_F^0$ , and  $\mu = 1 - u_{xc}(\infty)$  is the dimensionless Fermi energy of electrons accounting for the exchange-correlation interaction.

Unlike the analysis of validity conditions for the formula of induced density in homogeneous electron gas carried out in [10], which provides, along with (2.9), the estimate of critical density as  $R_{sc} = 5.64$ , in present case the dependence  $n_{ind}(u)$  is also affected by the quantum correction  $n_{qu}$  to the density. This influence is caused by the exchange-correlation potential in the local density approximation being dependent on the total electron density. For that reason, the analysis should be carried out all over again on the base of the expression

$$\frac{du}{dn_{ind}} = -\frac{2}{3}n_{ind}^{-1/3} - \frac{d}{dn_{ind}} [u_{xc}(n_{ind} + n_{qu})] \quad (2.25)$$

The result needed for qualitative understanding can be derived analytically, the correlation energy being neglected. Its consideration does not change the general picture, for even at the least acceptable value of density of the homogeneous electron gas at the infinity, corresponding to the highest acceptable value  $R_{sc} = 5.64$ , the ratio  $u_c(R_{sc})/u_x(R_{sc}) = 0.26$ , and the derivative ratio is even less,  $(du_c/dn)/(du_x/dn) \simeq 0.07$ . With a rise in density, these estimates still improve in the sense favorable to our purposes. At the same time, in the course of numerical realization of the algorithm the condition  $du/dn_{ind} \leq 0$  is easily checked without any simplification by the numerically known right-hand side of formula (2.25).

All the above considered, the inequality that determines the validity range of quasiclassical expression (2.7) is conveniently written as

$$-\frac{2}{3}n_{ind}^{-1/3} + \frac{1}{3}c_x R_s (n_{ind} + n_{qu})^{-2/3} \leq 0, \quad c_x = 2(2/3\pi^2)^{2/3} \quad (2.26)$$

The derivative of the exchange potential (2.8) is expressed here in our dimensionless variables. On the basis of (2.26) one can obtain the equation for critical values  $n_c$  of total density  $n = n_{ind} + n_{qu}$ , which correspond to changing in sign of the derivative  $du/dn_{ind}$ ,

$$n_c^2 - \beta n_c + \beta n_{qu} = 0, \quad \beta = (c_x R_s)^3/8. \quad (2.27)$$

Its solutions should satisfy the condition of non-negative total density,  $n \geq 0$ , and induced density,  $n_{ind} \geq 0$ , by virtue of their definition by formulae (2.5) and (2.7). The value of the quantum correction  $n_{qu}$  can be of any sign, because it is defined by formula (2.6) as a difference of two expressions for electron density found from the exact and approximate solutions of the Schrödinger equation.

The roots of equation (2.27) are given by

$$n_{c1,2} = \frac{\beta}{2} \left( 1 \pm \sqrt{1 - \frac{4}{\beta} n_{qu}} \right). \quad (2.28)$$

It is clear that with  $n_{qu} \leq 0$  only one root

$$n_{c1} = \frac{\beta}{2} \left( 1 + \sqrt{1 - \frac{4}{\beta} n_{qu}} \right), \quad (2.29)$$

satisfies the stated condition of non-negativity  $n_c$  and  $n_{ind}^{(c)} = n_c - n_{qu}$ . In the case of  $n_{qu} = 0$ , formula (2.29) gives the value of  $n_c$  for the homogeneous electron gas allowing for only the exchange potential, which after switching to atomic units corresponds to  $R_{sc} = 6.02$ . At



$n_{\text{qu}} < 0$ , the critical density is even higher. Taking into account the correlation potential also increases the estimate for  $n_c$ , adding a positive term to the left-hand side of inequality (2.26). In the case of a homogeneous gas with correlation energy as (2.9), this shifts the critical value towards  $R_{\text{sc}} = 5.64$ .

While negative values of  $n_{\text{qu}}$  do not change qualitatively the dependence of induced density  $n_{\text{ind}}$  on the average Coulomb potential  $u$  compared to the homogeneous case, leaving only one value of critical density, there is quite another picture at  $n_{\text{qu}} > 0$ . Both roots given by formula (2.28) have physical meaning and ensure positivity of both total density  $n_c$ , which is evident, and the induced one  $n_c - n_{\text{qu}}$ , which can be easily checked. It can also be seen that there is the limitation  $n_{\text{qu}} \leq \beta/4$  on the value of quantum correction to provide the existence of the roots. If  $n_{\text{qu}}$  exceeds this limit, the Coulomb potential  $u$  becomes a steadily decreasing function of  $n_{\text{ind}}$  in the total range of physically acceptable values, and the applicability condition (2.21) for the induced density formula (2.7) holds at any values of  $u$  and  $n$ .

It should be emphasized that the conditions for  $n_c$  caused by inequality (2.26) do not coincide with the condition of non-negativity of the radicand in formula (2.7), coming into action earlier. It is due to this circumstance caused by negativity of  $u_{\text{xc}}$  and its dependence on  $n$  that formula (2.7) breaks down earlier with growing potential  $u$ , than  $n_{\text{ind}}$  turns to zero. So at the increasing  $u$  or decreasing  $n$ , the induced charge drops to zero by a jump from some finite value in the course of iterations, creating discontinuities of the first kind in the distribution of total electron density and the effective potential, as can be seen in Fig. 1. After the self-consistency is achieved, this discontinuity naturally turns out to be less than accuracy specified, i. e. the loop termination criterion (2.20). Nevertheless, the treatment of this discontinuity when solving the Schrödinger and Poisson equations turned out an essential factor touching upon the effectiveness of the whole algorithm, what will be discussed further.

The estimate of the value of discontinuities in the density and effective potential can be made accurately, neglecting  $n_{\text{qu}}$ . It follows from the results of such analysis that the value of density discontinuity equals  $n_{\text{ind}}^{(c)}$ , taking on the value  $(R_s/R_{\text{sc}})^3$  at the initial cycle of iterations. One can see that with a growing non-ideality of electron gas and  $R_s$  closing to  $R_{\text{sc}}$  the dimensionless density jump tends to unity and becomes a more and more strong perturbation.

The discontinuity of effective potential equals  $u_{\text{xc}} [n_{\text{ind}}^{(c)}]$ , because the Coulomb potential is continuous everywhere. In the atomic units, this discontinuity has an universal value dependent only on the expression chosen for correlation energy and ranges from 0.1Ha with just the exchange potential taken into account to 0.15Ha with the correlation potential added according to the standard Wigner formula [2]. In the dimensionless units, however, the discontinuity of effective potential also grows considerably with the increase of electron non-ideality due to decreasing  $\varepsilon_{\text{F}}^0$ .

Now let us write down the algorithm of iterative solution for Eqs. (2.14)-(2.19) as applied to the case of semi-infinite many-electron systems with homogeneous positive background considered in this section, using the dimensionless variables introduced and duly commenting every step taken.

The initial value of the quantum correction to electron density and the total density itself are taken to be zero, and the initial position of critical point is taken beyond the boundary of positive background:

$$n_{\text{qu}}^0(\zeta) \equiv 0, \quad n^0(\zeta) \equiv 0, \quad \zeta_c^0 = \zeta_+ - 1. \quad (2.30)$$

Solving the Poisson equation (2.23), we find the Coulomb potential  $u^i$  satisfying the specified

boundary conditions and a new total electron density  $n_s^i$ , self-consistent with it,

$$n_s^i = n_{\text{ind}}^i + n_{\text{qu}}^i, \quad \zeta > \zeta_c^i, \quad n_s^i = n^i, \quad \zeta \leq \zeta_c^i, \quad i = 0, 1, \dots \quad (2.31)$$

In the process, a check for condition  $dn_{\text{ind}}^i/du^i < 0$  can show that critical point should be relocated to a new position  $\zeta_c^{i+1}$ . In the presence of functions  $n_s^i(\zeta)$  and  $u^i(\zeta)$  being numerically known, the simplest way of this check is to apply the formula (2.25), where  $n_{\text{ind}}^i$  is replaced with its expression in terms of potential  $u^i$  and definition (2.7) is rewritten in dimensionless variables:

$$n_{\text{ind}}^i = (\mu - u^i - u_{\text{xc}}(n_s^i))^{3/2}. \quad (2.32)$$

If critical point is shifted to the right, one should redefine  $n_s^i$ , replacing  $\zeta_c^i$  with  $\zeta_c^{i+1}$  in the procedure (2.31). Shift of the critical point to the left leaves  $n_s^i$  unchanged, though the new position of critical point defines the region of induced density formation after the Schrödinger equation has been solved.

The case of the initial cycle,  $i = 0$ , stands somewhat apart because the direct numerical solution of the second-order differential equation can be bypassed. Taking  $\zeta_c^0 = 0$ , one should begin the solution with Eq. (2.23). In the absence of the quantum correction to density, when the induced charge, nonlinear in  $u$ , does not depend explicitly on the coordinate  $\zeta$ , the first integral of this equation can be found in an explicit form. The solution is then found as numerical quadrature of the first integral. In that solving one determines the Coulomb potential  $u$ , the electron distribution self-consistent therewith and reduced here just to  $n_{\text{ind}}^0$ , and the critical point position  $\zeta_c^1$ . If the system as a whole is sufficiently described by quasiclassical approximation, such a solution may have a practical significance (see, for example, formulae (35.70)-(35.73) in [9] and the calculation of tunneling current through the Schottky barrier in [10]).

With the solution of the Poisson equation known, one can form the effective potential  $u_{\text{eff}}^i = u^i + u_{\text{xc}}^i(n_s^i)$  that enters into the Schrödinger equation. In virtue of translation invariance of the system under study in  $(x, y)$  plane, the total wave function can be written as

$$\Psi_{k, \mathbf{k}_{\parallel}}(\zeta, \mathbf{r}_{\parallel}) = \frac{1}{2\pi} e^{i\mathbf{k}_{\parallel}\mathbf{r}_{\parallel}} C \psi_k(\zeta), \quad (2.33)$$

where vector  $\mathbf{r}_{\parallel}$  lies in the  $(x, y)$  plane, and constant  $C$  is defined by the normalization requirement for function  $\psi_k$ . The Schrödinger equation for  $\psi_k^i$  at the  $i$ -th iteration cycle is conveniently written as

$$\frac{d^2}{d\zeta^2} \psi_k^i(\zeta) + (k^2 - u_{\text{eff}}^i(\zeta) + u_{\text{xc}}(\infty)) \psi_k^i(\zeta) = 0, \quad (2.34)$$

where the dimensionless quantum number  $k$  is normalized to  $k_F$ , and the scalar potential is calibrated by the condition  $u(\infty) = 0$ . An eigenvalue of  $k$  specifies the behavior of continuous spectrum eigenfunctions normalized to  $\delta(k - k')$  according to [2] (see formulae (24)-(25)) with the asymptotic form at infinity

$$\psi_k^i(\zeta) \rightarrow \sqrt{\frac{2}{\pi}} \sin(k\zeta + \gamma_k), \quad \zeta \rightarrow \infty. \quad (2.35)$$

The numerical solution  $\tilde{\psi}_k(\zeta)$  of the Cauchy problem for the homogeneous equation (2.34), found accurate within an arbitrary factor, is normalized correctly, if its asymptote at  $\zeta \rightarrow \infty$

is as Eq. (2.35). This is achieved multiplying the obtained solution by a constant  $A$  defined by relation

$$A^2 \left( \tilde{\psi}_k^2(\zeta_\infty) + \tilde{\psi}'_k{}^2(\zeta_\infty) \right) = 2/\pi. \quad (2.36)$$

Here  $\zeta_\infty \leq \zeta_{max}$  is a sufficiently remote point where potential  $u_{\text{eff}}(\zeta_\infty)$  can be considered as become a constant. The phase  $\gamma_k$  can be found from the relation

$$\gamma_k = \arctan \left[ k \frac{\tilde{\psi}_k(\zeta_\infty)}{\tilde{\psi}'_k(\zeta_\infty)} \right] - (k\zeta_\infty - l\pi), \quad (2.37)$$

where  $l = [k\zeta_\infty/\pi]$  is an integral part of the ratio. With such a definition, the phase is invariant with respect to the choice of  $\zeta_\infty$  point.

To conclude the  $i$ -th iteration cycle, the total electron density is calculated,

$$n^i(\zeta) = 3 \int_0^1 dk (1 - k^2) |\psi_k^i(\zeta)|^2 \quad (2.38)$$

as well as the quantum correction to the density for the next cycle

$$n_{\text{qu}}^{i+1}(\zeta) = n^i(\zeta) - n_{\text{ind}}(u_{\text{eff}}^i(\zeta)), \quad (2.39)$$

with the definition (2.32) taken into account.

The Cauchy problem for the Schrödinger equation was solved numerically using the fourth-order implicit technique that is often called the Numerov's method. The Numerov's algorithm does not include directly the value of first derivative of the sought solution specified at the initial point. Instead of this, one should know the value of the sought function at the first point from the boundary. To calculate this value with accuracy matching that of the Numerov's method, we represented the function as a second-order expansion in Taylor series. The necessary value of the second derivative at the boundary was found by means of the Schrödinger equation itself. A similar technique was applied to pass the discontinuities of effective potential. It has been checked within the chosen accuracy that the result of such a procedure is in accord with Runge-Kutta method commonly used to move one step away from the point where the Cauchy boundary conditions are specified.

The Poisson equation was solved by the relaxation method [11], its idea being to solve the matching nonstationary equation

$$\frac{\partial u}{\partial t} - \left( \frac{\partial^2 u}{\partial \zeta^2} + c_n n_{\text{ind}}(u, n_{\text{qu}}) \right) = -c_n [\theta(\zeta - \zeta_+) - n_{\text{qu}}(\zeta)] \quad (2.40)$$

instead of the stationary problem, until the solution stops changing in time  $t$  within the accuracy specified.

From the formal point of view, Eq.(2.40) is a nonlinear diffusion equation, a lot of numerical schemes having been developed for its solution. In present work we applied a scheme, in which, after discretization (2.40) in time with step  $\tau$  and in space with step  $h$ , one specifies an initial potential distribution satisfying the boundary conditions, and time evolution of the solution is monitored by solving the boundary value problem at each time point. As this takes place, one need not to obtain with a good accuracy the spatial distribution of potential  $u$  at each "time step", searching only for an accurate stationary solution at long times when change in  $u$  from step to step becomes small. The time discretization was made with an implicit first-order

scheme, so, when forming the boundary value problem at a new time point, the nonlinear term in the equation was estimated via the induced density  $n_{\text{ind}}(u, n_{\text{qu}})$  linearized in the increment of potential at the time step  $\tau$ . In the course of solving Eq. (2.40), the choice of  $\tau$  value was dictated, on the one hand, by considerations of numerical stability, and on the other hand, by those of computation speed (the time of reaching the stationary solution). In line with recommendations given in the literature, the initial time step was chosen according to relation  $\tau/h^2 = 0.1$ .

Since the linearization of dependence  $n_{\text{ind}}(u)$  was used at the movement from one time point to the next, the necessity could arise in the course of solving the Poisson equation to redefine the critical point to avoid the appearance of a region where  $dn_{\text{ind}}(u, n_{\text{q}})/du > 0$ . This was carried out similarly to the procedure described after formula (2.32). As noted above, the magnitude of ordinary jump of the electron density increases with  $R_s$  and leads to more and more violent perturbations of numerical solution. It was found (see details in Sec. 4) that at  $R_s \lesssim R_{\text{sc}}$  the convergence of solution of the equation set (2.14) - (2.19) deteriorates. It appears though to be rather a consequence of some specific numerical algorithm realization, than a drawback of the iteration scheme suggested.

### 3 Properties of electron gas in the barrier structures

In this section, we apply our method of solving the Kohn-Sham equations to finding the self-consistent electron density and effective potential in a barrier structure that consists of two conductors with degenerate electron gas separated by an insulating layer with dielectric permeability  $\kappa_{\text{d}}$ . We assume that z-axis is perpendicular to the layer plane, the conductors are positioned at  $z \leq -d/2$  and  $z \geq d/2$  respectively, and the insulating layer lies at  $|z| < d/2$ . It is assumed further on that the neutralizing background in the conductors is homogeneous, and the barrier is not impurity-doped, that is,

$$N_+(z) = \begin{cases} 0, & |z| < d/2, \\ N_+, & |z| \geq d/2. \end{cases} \quad (3.1)$$

The height of potential barrier formed by the insulator is taken to be infinite, so that wave functions turn to zero at the conductor-insulator interface.

#### 3.1 Self-induced energy levels in semiconductors

In the case of infinitely high potential barrier, the electron states localized in  $z$  and the size-quantized two-dimensional subbands can emerge even if inhomogeneities of positive background  $N_+(z)$  and applied voltage are absent. The existence of such states was suggested for the first time in [12], where the discrete energy levels in question were called "the plasma levels". The appearance of localized states was attributed to the electron wave functions turning to zero at the barrier interface. Due to continuity of wave functions, the electron density close to the barrier is small and inadequate to provide the local neutrality. The uncompensated positive charge near the interface creates a self-consistent potential well, wherein bound states can exist. According to calculation carried out in [12] for the case of degenerate electron gas, the discrete levels should exist at  $R_s \leq 2.87$ , while at  $R_s \leq 0.15$  the second bound state appears in the near-barrier well.

Independently of [12], the idea of depletion region near the barrier was also suggested in [13], where the energy of localized states and the depth of self-induced potential well were calculated as functions of  $R_s$ . However, in these works either the self-consistency has not been reached, as in [12], or some model potential was used in the Schrödinger equation instead of the exact solution of Poisson equation [13]. The exchange-correlation interaction of free charge carriers was neglected in both papers. The self-induced levels are quite shallow with energies less than 0.1 of the potential well depth ( $\simeq 2$  meV for a semiconductor with n-GaAs parameters), thus being very close to the states of continuous spectrum. A small change in the potential well shape can make them disappear. In this context, it was interesting to find out if these states remain in the self-consistent solution.

The Kohn-Sham set of equations was solved according to iteration scheme (2.14) - (2.19). The total dimensionless electron density  $n^i$  at  $z \geq d/2$  obtained after solving the Schrödinger equation on the  $i$ -th iteration was calculated by formula

$$n^i(\zeta) = 3 \int_0^1 dk (1 - k^2) |\psi_k^i(\zeta)|^2 + \frac{3\pi}{2} \sum_j |\psi_j^i(\zeta)|^2 (1 - \varepsilon_j^i), \quad (3.2)$$

where  $\zeta = k_F(z - d/2)$ ,  $j$  is the number of a discrete level,  $\varepsilon_j$  are discrete energy levels,  $\psi_k$  and  $\psi_j$  are the respective wave functions of continuous and discrete parts of the spectrum. The first term in (3.2) corresponds to the density of continuous-spectrum electrons, and the second one is the electron density in the localized states.

Since the considered problem with an infinitely high barrier is close to that of potential scattering of  $s$ -wave by a short-range potential, one could search for energy levels in the potential well by means of the Levinson's theorem (see, for example, [14]) that expresses the number  $m$  of levels in a well in terms of the asymptotic phase (2.35) of continuous-spectrum wave functions at infinity by relation  $\lim_{k \rightarrow 0} \gamma_k = m\pi$ . Although this formula is used, for example, in [15] for a theoretical analysis of barrier structure, it is not convenient in numerical calculations because of redundant computation of wave functions for empty states. Instead of this, it suffices to find a solution of the Schrödinger equation (2.34) at  $k = 0$  and calculate the number of zeros within the interval  $0 < \zeta < \infty$ .

However, when finding the energy and the wave function of a bound state we applied the trigonometric sweep method, which eliminates the well-known numerical instability of solution decreasing in the classically forbidden region, caused by the second solution that grows exponentially [16]. In this method, the wave function is written as

$$\psi(\zeta) = a(\zeta) \sin \eta(\zeta), \quad \frac{d\psi}{d\zeta} = a(\zeta) \cos \eta(\zeta), \quad (3.3)$$

so one can easily show that the total phase  $\eta(\zeta)$  introduced here has the increment  $\pi$  at zeros of the function  $\psi(\zeta)$  where the logarithmic derivative of the latter turns to infinity. There are two first-order equations for the phase and the amplitude

$$\frac{d\eta}{d\zeta} = (\varepsilon - u_{\text{eff}}(\zeta) + u_{\text{eff}}(\infty)) \sin^2 \eta + \cos^2 \eta \quad (3.4)$$

$$\frac{da}{d\zeta} = \frac{1}{2} a \sin 2\eta (1 + u_{\text{eff}}(\zeta) - u_{\text{eff}}(\infty) - \varepsilon), \quad (3.5)$$

which are derived from (2.34) taking (3.3) into account. The equation for  $\eta(\zeta)$  is solved with initial condition  $\eta(0) = 0$ , while the initial condition for the amplitude can be taken at random

and specified definitely by the wave function normalization to 1. The level energy  $\varepsilon_j \leq 0$  corresponds to the limit value of phase  $\eta_\varepsilon(\infty) = j\pi, (j = 1, 2, \dots)$ . So to calculate the number of levels in a well, one should only solve the equation (3.4) for two energy values corresponding to the potential well bottom and the edge of continuous spectrum  $\varepsilon = 0$ , and find the  $\pi$  multiplicity of the difference between the two phases at infinity.

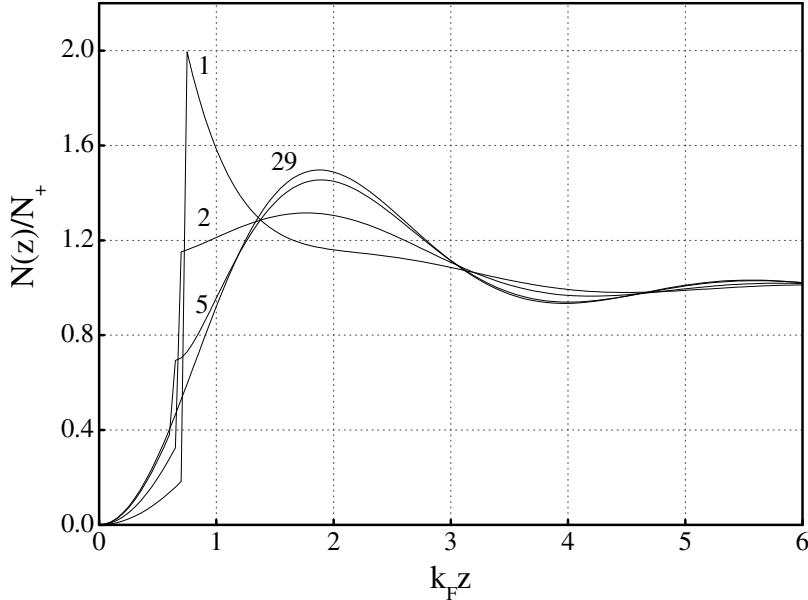


Figure 1: Electron density obtained at various cycles of iteration process. Number of curve corresponds to the number of iteration after which it was calculated. In this section, coordinate  $z$  in the figures is counted from the point  $d/2$ .

Boundary conditions for the Poisson equation were taken as

$$\left. \frac{du}{d\zeta} \right|_{\zeta=0} = 0, \quad \left. \frac{du}{d\zeta} \right|_{\zeta=\infty} = 0. \quad (3.6)$$

Note that such boundary conditions along with Fermi level specified by the requirement of local neutrality at  $\zeta \rightarrow \infty$  and the choice of  $u(\infty) = 0$  define a unique numerical solution of the Poisson equation (2.23) and ensure its tending to zero at infinity.

Fig.1 demonstrates the electron density distributions obtained by various number of iterations. One can easily see that, at the initial iterations, the spatial dependence of electron density has discontinuities at the boundary of validity of quasiclassical expression for induced charge in the form (2.7). The discontinuities disappear in the course of iteration process, and final self-consistent density is a smooth function of coordinate. It is also essential to note that iteration convergence criteria specified were usually reached at 10-14 cycles (depending on  $R_s$ ). The continued calculations did not provide a noticeable increase in accuracy at chosen discretization parameters, but neither disrupted the solution, as can be seen from Fig. 1, which testifies to the stability of the algorithm applied.

Fig. 2 demonstrates the coordinate dependence of the self-consistent potential and electron density. As can be seen from Fig. 2A, taking into account the  $U_{xc}$  modifies shape and depth of the potential well and, correspondingly, the energy of localized state (see curves 1 and 2 in

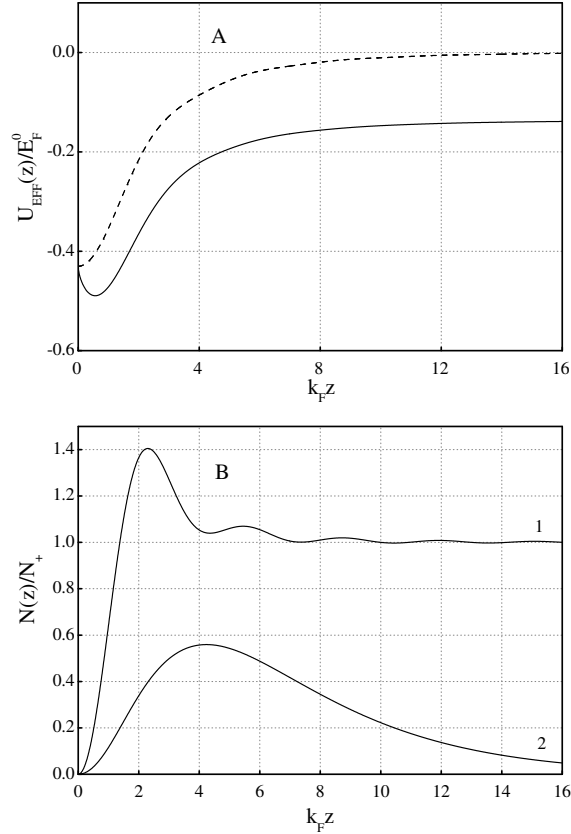


Figure 2: Self-consistent potential and electron density at  $R_s = 0.4$ . Fig. 2A demonstrates the self-consistent potential with account of the exchange-correlation interaction (solid line) and that in the Hartree approximation (dashed line). Fig. 2B shows the total self-consistent electron density (curve 1) and density of electrons localized in the size-quantized subband (curve 2).

Fig. 3). The total self-consistent electron density in Fig. 2B (curve 1) is the sum of density of electrons in the size-quantized subband (curve 2) and that of electrons in the continuous spectrum states. Localized electrons are concentrated mainly close to the potential barrier, though the localization pattern depends on  $R_s$ .

The  $R_s$  dependencies of self-consistent well depth and energy of the state localized therein are presented in Figs. 3A and 3B respectively. Curves 1 and 2 in both figures are results obtained in present work, while curves 3 and 4 are results presented in papers [12] and [13]. One can see that calculated level energy and its  $R_s$  dependencies presented in [12] (curve 3B) differ both quantitatively and qualitatively from our self-consistent calculations. Furthermore, we did not find two localized levels in the potential well in the absence of external electric field at any values of  $R_s \geq 0.05$ . The second level with a dimensionless cohesive energy about 0.0016 was found only at  $R_s = 0.005$  that is not, as a rule, realized physically in real structures. Nevertheless, one should note that the idea of a self-consistent potential well with bound states close to infinitely high barrier, put forward in [12], proved to be true.

The results reported in [13] for the potential well depth are in rather good agreement with the self-consistent calculation of the present work in the Hartree approximation (see. curves 2 and 4 in Fig. 3A). However, the energy of bound state (curve 4 in Fig. 3B), calculated in [13] differs from the accurate solution both in magnitude and the  $R_s$  dependence, particularly at

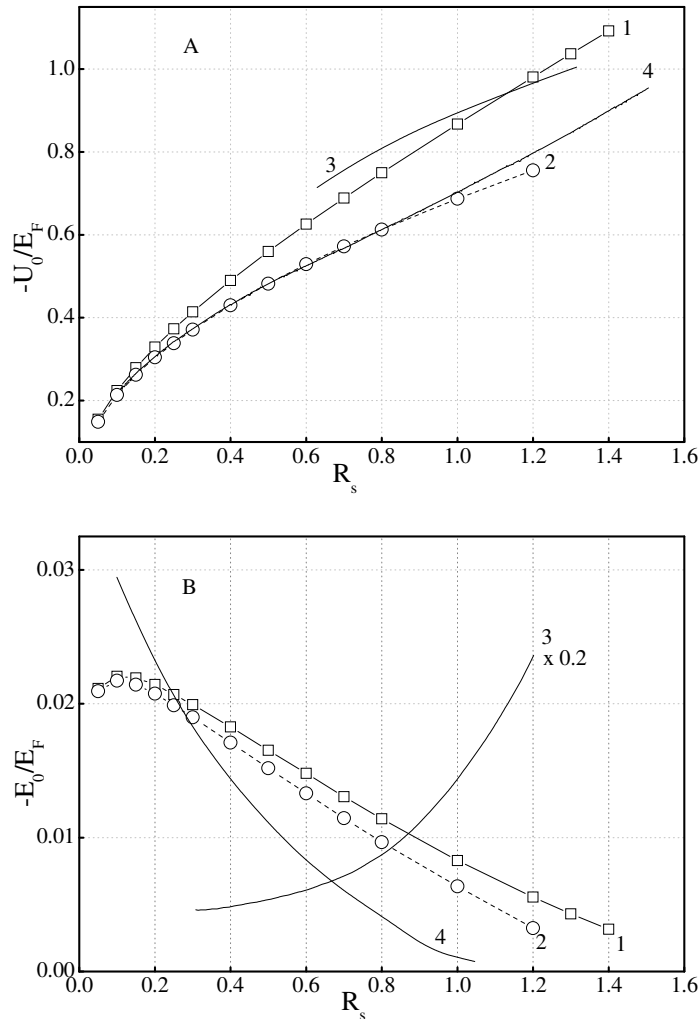


Figure 3: Potential well depth (A) and bound-state energy (B) as functions of  $R_s$ . Curves 1 were calculated with account of the exchange-correlation interaction, curves 2 are results of self-consistent calculation in the Hartree approximation. Curves 3 and 4 represent results presented in [12] and [13] respectively.

small values of this parameter. At the same time, the difference cannot be attributable to the exchange-correlation interaction neglected in [13], as it is evident from the relative closeness of our curves 1 and 2 in Fig. 3B to each other.

It may be safely supposed that considerable error in the self-consistent energy levels found by method used in [13] is caused by inaccurate description of the potential well shape by a three-parameter model potential.

Taking into account the finite barrier height leads to a change in boundary condition for electron wave functions at the insulator/conductor interface, and that, as calculation shows, leads in its turn to a lowering upper limit of  $R_s$  region where localized states are observed. At a considerable decrease of barrier height the discrete level disappears entirely.

Far from potential barrier,  $k_F z \gg 1$ , the effective potential and electron density manifest the Friedel oscillations (see. Fig. 4). One can see that the oscillation amplitude of effective potential with  $U_{xc}$  component is considerably less than that of Coulomb potential. Such suppression



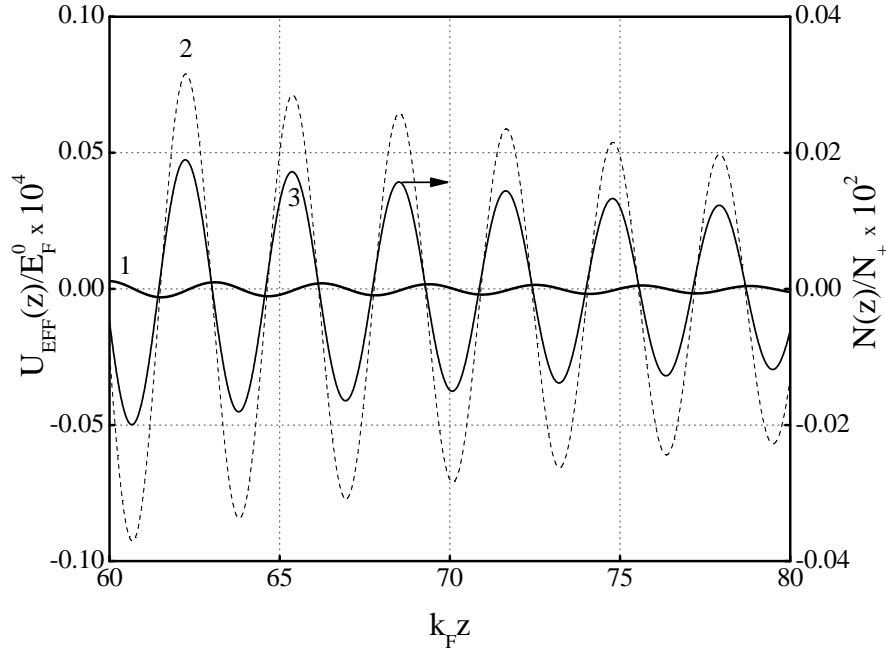


Figure 4: Friedel oscillations of effective potential and electron density in the electron gas limited by an infinitely high barrier. Curve 1 is effective potential, curve 2 is the Coulomb component of effective potential, curve 3 is electron density

of oscillations can be understood as follows. According to Poisson equation, the oscillating component of electron density is maximal at the same points as the Coulomb potential. The exchange-correlation contribution into  $U_{\text{eff}}$  always has a sign opposite to that of the direct interaction. So in virtue of the repulsive nature of electron-electron interaction, the potential  $U_{\text{xc}}$  is negative, and its magnitude grows steadily with electron density according to formulae (2.4), (2.8) and (2.11). Consequently, at the points of maximum Coulomb potential the exchange-correlation contribution is also maximal in magnitude and negative.

The similar considerations show that at the minima of the effective potential the Coulomb contribution and the exchange-correlation one also summarize in phase opposition. As long as the relative role of  $U_{\text{xc}}$  grows with decreasing electron density, this leads to the oscillation magnitude of effective potential being suppressed more than that of the Coulomb one with growing  $R_s$ . Note that the influence of  $U_{\text{xc}}$  upon the  $R_s$  dependence of oscillation magnitude of the dimensionless electron density is quite opposite. The reason for this is discussed in more detail in Section 5.

In conclusion, one should note that the system considered with filled states of discrete and continuous spectrum has much in common with quasi two-dimensional electron gas of accumulation layers close to semiconductor-insulator boundary with an external electric field applied or even without it. Though one believes [17] that the problem of self-consistent spectrum calculation for size-quantized subbands in the enriched layer is solved in [15], publications concerned with methods for calculating such structures still appear [18]. However, as before, no proved technique is suggested allowing to avoid the mismatch between the total charge or the dipole moment of quasi two-dimensional gas obtained at intermediate steps of iteration and boundary conditions to Poisson equation imposed on the potential. To make a solution possible, the authors renormalize the electron density found by means of the Schrödinger equation, and

also vary the Fermi level position in the bulk of semiconductor. The results obtained in the present section of our work make clear that the algorithm suggested allows one to obtain the solution in a regular manner within the framework of mathematically complete and accurate iteration procedure.

### 3.2 The capacitance limitation of a barrier structure

Up to now it was assumed that external voltage is not applied to barrier structure. In this section, we find the self-consistent distribution of electron density and effective potential in the case of a dc bias  $V$ , and calculate the capacitance of the barrier structure. Apart from the check for the algorithm performance, this problem is of independent interest in connection with the capacitance limitation of thin-film capacitors in general, posed in [19], as well as with particular case of nanocapacitor with a thin-film ferroelectric insulator in view of its application prospects in electronics [20].

It was shown by Mead [19] that the measured inverse capacitance of the metal-insulator-metal junction as a function of insulation layer thickness  $d$  does not tend to zero at  $d \rightarrow 0$  in contrast to the common formula for geometrical capacitance of a plate capacitor. This was explained qualitatively by the finite thickness of the spatial charge layer that screens the electric field penetrating the real metal. The quantitative analysis of this situation in the framework of the Thomas-Fermi approximation for electrons in the metal was carried out in [21] and complemented with an account of dielectric permeability of the metal electrode in [22]. In the latter work, it was also noted that using the insulator with a high permeability  $\kappa_d$  makes the effect of non-ideality of electrons more pronounced even at insulator thickness much greater than the Thomas-Fermi screening length in the electrodes, and the maximum achievable junction capacitance with given electrodes was introduced as the limit at  $\kappa_d \rightarrow \infty$ .

The formulae for capacitance obtained in the above papers provided a qualitative understanding of its experimental dependence on the material of electrodes and insulator, and also allowed one to get a correct order-of-magnitude estimate for the contribution of spatial charge region to the capacitance. However it was noted that the effect of the exchange-correlation interaction of electrons in metal and that of the charge in the Friedel oscillations of the density are still unclear and cannot be accounted for in terms of the Thomas-Fermi approximation. At the same time, as early as in work [23] by Bardeen it was actually shown that spatial electron redistribution related to the density oscillations caused by the barrier does not keep the total neutrality of the system because of the occurring deficit of electron charge. In the case of an infinitely high barrier without an external field applied this charge deficit equals (in the approximation of non-interacting electrons)

$$\int_0^{\infty} dz (N(z) - N_+) = -\frac{k_F^2}{8\pi}, \quad (3.7)$$

which coincides with the excess of the positive charge given by formula (26) in [23] (with printing error corrected, see. Eq. (2) in [24]). Besides, it follows from the results of previous section that self-induced surface level also can capture a considerable electron charge (see. Fig. 2B). With a noticeable field dependence of charge in the oscillations and on the near-barrier level their contribution to the capacitance may be comparable with that of the charge in the Thomas-Fermi screening region.

All above factors can be estimated by solving self-consistently the Kohn-Sham equations for a barrier structure in the jellium model. Let us consider a system of two semi-infinite metals separated by the infinite potential barrier of width  $d$  and dielectric permeability  $\kappa_d$ . Such a barrier prevents the charge transfer between two parts of the system when voltage is applied. The differential electrostatic capacitance per unit area of a wholly neutral system is given in terms of the charge  $Q$  per unit area of the right-hand side of the structure by formula

$$C(V) = -\frac{dQ}{dV} = \frac{d}{dV} \int_{z_0}^{\infty} dz(N(z, V) - N_+(z)), \quad (3.8)$$

where  $V = \varphi(-\infty) - \varphi(\infty)$  is voltage across the structure equal to the work done by the electric field on a unit positive charge to move it from negative to positive infinity. Here  $\varphi(z)$  is the dimensional Coulomb potential. The point  $z_0$  given by  $dD/dz|_{z_0} = 0$  is the sign changing point of charge density in the region where electric induction  $D$  is maximal. As long as electric field is zero at both infinities because of the finiteness of potential  $\varphi(z)$ , the definition (3.8) provides that charges in two parts of the structure are equal in absolute magnitude.

We assume that the metal electrodes are identical and the positive background distribution is described by formula (3.1). To simplify calculation, we also neglect a possible nonzero value of the contact potential difference along with related built-in fields and charges in surface states, as it was assumed in the model considered in [21] and [22]. These conditions mean the absence of charge within the barrier, which allows one to take any point of the insulator as  $z_0$  including the boundary ones  $z_0 = \pm d/2$ . If the induction  $D$  inside the barrier is specified, the right-hand electrode charge equals

$$Q(V) = -D/4\pi. \quad (3.9)$$

We represent the voltage across the total structure as a sum of voltages across its three constituent parts,

$$V = [\varphi(-\infty) - \varphi(-d/2)] + E_d d + [\varphi(d/2) - \varphi(\infty)], \quad (3.10)$$

where field inside the barrier  $E_d = D/\kappa_d$ . Let  $\varphi_{\pm}(z, E)$  be the Poisson equation solutions at  $d/2 \leq z \leq \infty$  and  $-d/2 \geq z \geq -\infty$  with boundary conditions  $d\varphi_{\pm}/dz|_{z=\pm d/2} = E$ ,  $\varphi_{\pm}(\pm\infty) = 0$  respectively. Then, in view of induction continuity at the insulator-metal boundary, the equality (3.10), can be rewritten as

$$V = -\varphi_-(-d/2, D/\kappa_m) + E_d d + \varphi_+(d/2, D/\kappa_m). \quad (3.11)$$

Let  $E_m = D/\kappa_m$  be the field in metal at the insulator interface, where the not-equal-to-one dielectric polarization  $\kappa_m$  takes into account a possible polarizability of internal electron shells of ion cores. Since in our case  $\varphi_-(-d/2, E_m) = \varphi_+(d/2, -E_m)$ , we get a resulting formula, which reduces the calculation of barrier-structure capacitance to the problem for semi-infinite system considered in the previous section,

$$V = \varphi_+(d/2, E_m) - \varphi_+(d/2, -E_m) + E_d d. \quad (3.12)$$

We calculate the capacitance at small voltage when differentiation in Eq. (3.8) can be replaced with the ratio of small increments. Due to the additive structure of  $V$  in (3.12), it is more convenient to deal with the inverse capacitance. Taking (3.9) into account, we get

$$C^{-1} = -\frac{V}{Q} = 4\pi \frac{\varphi_+(d/2, E_m) - \varphi_+(d/2, -E_m)}{\kappa_m E_m} + 4\pi \frac{d}{\kappa_d} \equiv 2C_i^{-1} + C_d^{-1}, \quad (3.13)$$

where the standard notation  $C_i$ ,  $C_d$  is used at the end for separating contributions of voltage across the interfaces (inside the metal electrodes) and the insulator to the total capacitance. The explicit definition for  $C_i$  and  $C_d$  can be easily seen from the structure of expression (3.11), if one takes into account that  $\varphi_+(d/2, 0) \neq 0$  (see. Fig. 2A). It is evident that the maximal possible capacity  $C_{\max}$  of the considered structure is achieved in the limit of small electric thickness of insulator,  $\lim d/\kappa_d \rightarrow 0$ , and can be written as

$$C_{\max}^{-1} = 4\pi \frac{\varphi_+(d/2, E_m) - \varphi_+(d/2, -E_m)}{\kappa_m E_m}. \quad (3.14)$$

We assume further on that  $\kappa_m = 1$ , for, as may be required, the numerical value of capacitance being found can be easily recalculated using Eq. (3.14) and taking into account the relevant redefinition of atomic units.

The structure of formula (3.14) shows that, for calculating the capacitance limitation of barrier structure one should solve twice the problem for semi-infinite metal bounded by an infinitely high barrier with boundary conditions as

$$\left. \frac{du}{d\zeta} \right|_{\zeta=0} = \pm E, \quad \left. \frac{du}{d\zeta} \right|_{\zeta=\infty} = 0. \quad (3.15)$$

Here we use the dimensionless variables for electron potential energy and spatial coordinate introduced in Section 2.2. The dimensionless electric field  $E$  is normalized to intrinsic field  $E_c = k_F \varepsilon_F^0 / e$ . Apart from the change in the boundary condition at zero compared to (3.6), no modifications were needed in the calculation program.

The found values of potential at the insulator boundary at two values of electric field were used in formula (3.14) for capacitance calculation. For the purpose of accuracy and to verify that the chosen field magnitudes are sufficiently small and do not exceed the limits of linear voltage dependence of the charge, the potential was calculated for three pairs of values  $\pm E$ , and the slope of the linear dependence obtained was used to calculate the capacitance.

Fig. 5 demonstrates the  $R_s$  dependence of capacitance limitation (denoted just as  $C$ ) of the structure obtained in different approximations. Curves 1 and 2 correspond to the self-consistent calculation of capacitance with account of the exchange-correlation interaction and in the Hartree approximation. Curve 3 was obtained in the Thomas-Fermi approximation and can be represented by a simple explicit formula

$$C = \frac{k_{\text{TF}}}{8\pi} = \frac{1}{8\pi} \left( \frac{12}{\pi} \right)^{1/3} \frac{1}{R_s^{1/2}}, \quad (3.16)$$

where  $k_{\text{TF}}$  is the inverse Thomas-Fermi length. If, in the Thomas-Fermi approximation, we also take into account the exchange-correlation potential in accordance with formula (2.7), we get the capacitance formula like (3.16), but with  $k_{\text{TF}}$  replaced with renormalized value  $\tilde{k}_{\text{TF}} = k_{\text{TF}} / (1 + \frac{3}{2} du_{xc}/dn)^{1/2}$ . The corresponding curve is not shown in Fig. 5 because the difference between these two curves in the considered range of  $R_s$  is almost just as small as between curves 1 and 2. With an exact calculation, the account of exchange-correlation potential leads to the decrease of capacitance, which is probably related to withdrawal of the minimum of self-consistent potential well and charge accumulated therein from the barrier (see Fig. 2a).

The comparison of numerical values of interface capacity  $C_i = 2C$  obtained from curve 1 with its experimental estimations (see, for example, [25]) shows an agreement in the order of magnitude. Thus, not taking into account the dielectric permeability of electrode metal,

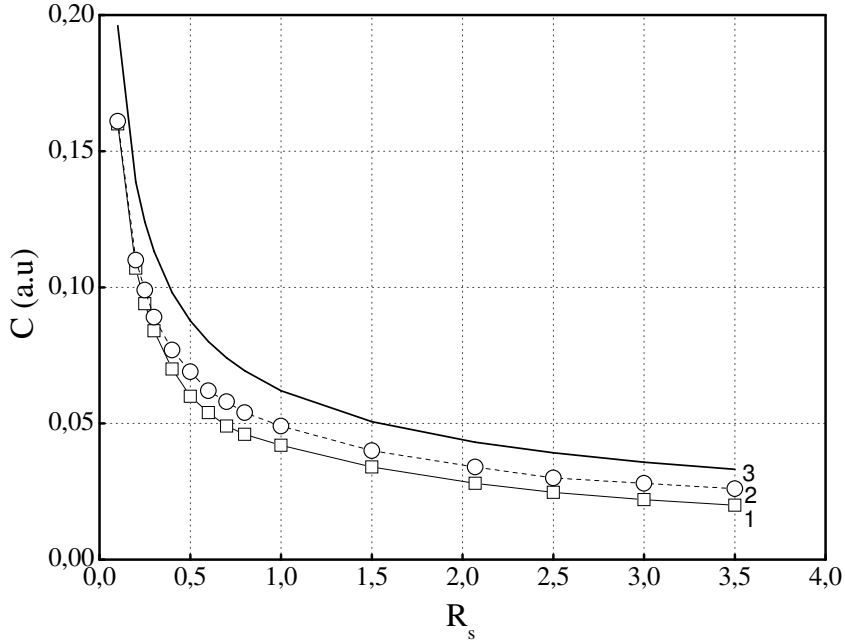


Figure 5: Capacitance of barrier structure at various values of  $R_s$ . Curve 1 is self-consistent calculation with account of exchange-correlation interaction, curves 2 and 3 are the same in the Hartree and Thomas-Fermi approximations respectively.

which differs noticeably from unity for the noble [26] and transition [27] metals, the range of  $C_i$  change, according to curve 1 in Fig. 5, is from 275 to 85 fF/ $\mu^2$  at  $0.5 \leq R_s \leq 3.5$ . In terms of the effective electric thickness  $d_{\text{eff}} = (4\pi C_i)^{-1}$  we get the range from 0.035 to 0.11 nm. The analysis of current theoretical and experimental data made in [28] led to the conclusion in favor of imperfect screening in metal contacts as the main reason for the so-called "dead layer" observed experimentally. The latter determines the maximum achievable capacitance in structures with ferroelectric insulator for a specified choice of metal for electrodes.

The general conclusion from the data presented in Fig. 5 is that the Thomas-Fermi approximation with its exponential distribution of spatial charge does provide the order-of-magnitude agreement with complete self-consistent calculation as concerns the capacitance limitation. Neither the exchange-correlation interaction of electrons, nor density oscillations or an account of the self-induced potential well with a discrete energy level therein prove essential. The level that appeared at  $R_s < 1.6$  did not affect the smoothness of the curve  $C(R_s)$ , in accordance with result reported in [29]. The similar absence of drastic changes in the experimental curve  $C(V)$  at changing number of size-quantized levels in the accumulation layer of  $n - InAs$  was reported in [30].

In work [15], the preservation of continuous dependence of self-consistent well potential on the external electric field regardless of the bound state appearance or disappearance was explained by forming of an "orthogonal hole" in the spatial distribution of electrons filling the states of continuous spectrum. Our numerical results demonstrate that this phenomenon is determined by appearance or disappearance of one more zero in the continuous-spectrum wave functions with the appearance or disappearance of a bound state in the potential well. As a consequence, filling of a bound state is accompanied, in a sense, by redistribution of total electron density among its two components in formula (3.2), rather than contribution

from the level is added to the existing one from the continuous spectrum. On the contrary, failing to account for (or neglecting) the contribution from a bound state, even quite shallow, in the iteration process leads to formation of a shallow and wide potential well with more levels appearing at the next iteration cycle, so the iteration process fails to converge.

## 4 Work function and surface energy density of metal in the model with homogeneous background

In the model with homogeneous positive background (jellium model), the metal work function and surface energy density were calculated in a good many papers. However, the existing data reveal sometimes not only quantitative, but also qualitative difference. We believe that the reason for such divergence is related to the complete self-consistence being not reached in the works under discussion when calculating the distribution of electron density and effective potential. Among the detailed and comprehensive works with calculation technique described one could mention publications [3], [31] and [32], our results we will compare with. Note that the purpose of this part of our work is to obtain an actually self-consistent solution for one of the classical problems of the theory of inhomogeneous electron gas and assess the importance of self-consistency by comparing the results with those obtained by other methods for the same problem statement. We do not aim at improving the jellium model or the density functional theory for calculating the surface properties of metals.

The problem statement here is generally similar to calculation of barrier structure properties considered in the previous section. However, in the case of metal the surface barrier is formed entirely by the self-consistent field and does not contain any specified seed potential. Besides, in metals in ordinary conditions, the values of  $R_s$  calculated for charge carriers with free electron mass in the medium with dielectric permeability  $\kappa_m = 1$  exceed considerably  $R_s$  values typical for semiconductor structures and lie in the range  $2 < R_s < 5.7$ . All the above raised the interest for a calculation intended to explore the behavior of convergence to the self-consistent solution and assess the algorithm stability at  $R_s$  values exceeding those considered in Section 3.

### 4.1 Work function of simple metals

Let the positive background occupy the half-space  $z > z_+$  where  $z_+$  is coordinate value at the metal-vacuum boundary. In the calculation, the boundary conditions for the Poisson equation (2.23) were taken as  $du/d\zeta|_{\zeta=\pm\infty} = 0$ . Wave functions  $\psi_k(\zeta)$  of single-particle states with energies not exceeding the Fermi level were found as Cauchy problem solutions exponentially damped at  $\zeta \rightarrow -\infty$  and normalized according to Eqs. (2.33) and (2.35). The dimensionless work function  $w = W/\varepsilon_F^0$  (see Fig. 6) equals the potential barrier height counted from the value of bulk chemical potential,

$$w = u_{\text{eff}}(-\infty) - \mu.$$

The self-consistent electron density and effective potential obtained after convergence of iteration process in accordance with calculation scheme described in Section 2 are shown in Fig. 6. The curves  $n$  and  $u_{\text{eff}}$  taken from the table 1 in the work [3] are presented by dots in the same figure for comparison. One should note that in work [3] the correlation energy was taken as standard Wigner formula

$$\varepsilon_c = -\frac{0.44}{R_s + 7.8}, \quad (4.1)$$

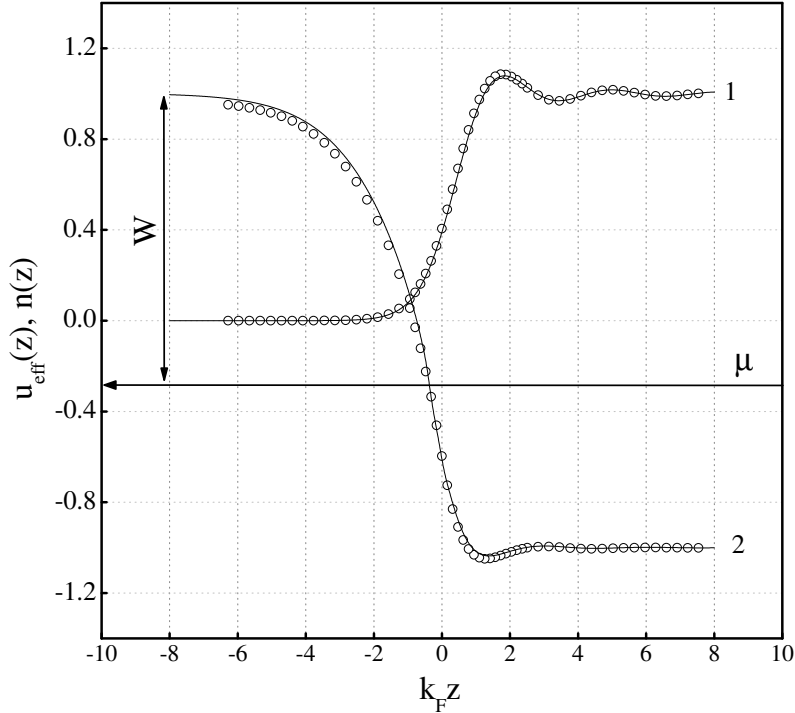


Figure 6: Comparison of self-consistent calculation for effective potential and electron density (solid curves) in present work with similar data from work [3] (points) at  $R_s = 4$ .

rather than expression (2.9) used in present work. For the correct comparison, the result of our self-consistent solution presented in Fig. 6 was calculated using correlation energy (4.1). One can see that calculation results in the figure agree rather well, though in work [3] a 12-parameter formula for electron distribution was used instead of searching for self-consistency, and those parameters were found by some variational procedure (see. Appendix B in [3]).

However, the convergence of our iteration solution and its good agreement with the generally accepted calculation results from the work [3] by Lang and Kohn at a particular value of  $R_s$  are not in themselves sufficient for a full assessment of the self-consistency degree achieved. In the work [33] within the model of homogeneous background, an universal relation for electrostatic potential was obtained,

$$U(z_+) - U(\infty) = N \frac{d\varepsilon}{dN} \equiv \tilde{\Delta}_{\text{BV}}, \quad (4.2)$$

where  $\varepsilon$  is total energy per one electron in homogeneous electron gas. For further convenience, we introduce the dimensionless parameter of self-consistency  $\Delta_{\text{BV}} = \tilde{\Delta}_{\text{BV}}/\varepsilon_{\text{F}}^0$  and write it as

$$\Delta_{\text{BV}} = \frac{2}{5} + 2 \left( \frac{4}{9\pi} \right)^{2/3} R_s^2 [U_{\text{xc}} - \varepsilon_{\text{xc}}], \quad (4.3)$$

where the expression in square brackets is left in atomic units. The relationship (4.3) was used to verify if the calculated potential is actually self-consistent with the electron density. Good agreement between  $\Delta = u(\zeta_+) - u(\infty)$  and  $\Delta_{\text{BV}}$  proves that a genuine self-consistent solution of the Kohn-Sham equations was found (see. [33], p. 1430). The Table 1 presents the values of  $\Delta$  and parameter  $\Delta_{\text{BV}}$  corresponding to the results of self-consistent calculation

Table 1: The  $R_s$  dependence of parameters  $\Delta$  and  $\Delta_{\text{BV}}$  as well as work function  $W$  and surface energy density  $\Sigma$ . The number of iterations needed to reach self-consistency is also presented.

$R_s$	$\Delta$	$\Delta_{\text{BV}}$	$W$ (eV)	$\Sigma$ (erg/cm <sup>2</sup> )	$N_{\text{iter}}$
0.3	0.3751	0.3751	3.12	-	12
0.5	0.358	0.358	3.21	-	8
1.0	0.317	0.317	3.40	-	6
1.3	0.291	0.291	3.51	-	6
1.5	0.274	0.274	3.60	-	7
1.65	0.261	0.261	3.63	-	7
1.8	0.248	0.248	3.64	-	7
2.07	0.224	0.224	3.60	-1340	9
2.3	0.204	0.204	3.53	-583	8
2.5	0.186	0.186	3.48	-321	12
3.28	0.115	0.115	3.12	106	9
3.99	0.051	0.051	2.87	71	17
4.96	-0.047	-0.047	2.50	65	28

for specific  $R_s$  and  $\varepsilon_c$  values in accordance with formula (2.9). One can see that  $\Delta$  and  $\Delta_{\text{BV}}$  match for all  $R_s \leq 3.99$  to an accuracy better than 0.001. Contrary to work [32] where the criterion (4.2) was used explicitly in the process of solution building, this relationship is never taken into account in our algorithm. So its satisfaction proves that  $n$  and  $u_{\text{eff}}$  obtained are genuine self-consistent solutions of Kohn-Sham equations for assumed approximation for the exchange-correlation potential of electrons.

One should note the sensitivity of the self-consistency criterion to the values of potential at the positive background frontier. The degree of agreement between  $\Delta$  and  $\Delta_{\text{BV}}$  presented in Table 1 is achieved only if the potential  $u(\zeta_+)$  value taken is interpolated to the discretization half-step  $\delta\zeta$  towards vacuum region. In the calculation,  $\delta\zeta$  was chosen within the interval  $0.05 \div 0.005$ .

A similar self-consistency test for electron density and potential found by Lang and Kohn [3] was carried out in the work [33]. The data presented there in Table 1 show that, even in the case of improved (unpublished) results of Lang, the self-consistency criterion (4.2) is fulfilled to an accuracy better than the third decimal place only for  $R_s \leq 4$ . With growing  $R_s$  the agreement is steadily worsening and at  $R_s = 6$  the deviation reaches 0.01. This means that at large values of  $R_s$  close to the existence limit of real metals, the parametrization scheme chosen in work [3] and the method of calculating the parameters are not quite an adequate replacement for an accurate solution of the Kohn-Sham set of equations. This fact can be considered as an indication of serious difference in the behavior of electron density and potential at the  $R_s$  values close to critical  $R_{\text{sc}}$ , from the jellium model solutions at higher densities of electron gas, which was discussed in some measure in Section 2.

It follows from the Table 1 that in our calculations at  $R_s \simeq 5$  the self-consistency criterion is also fulfilled worse than at small values. In the region  $R_s \leq 3.99$ , the iteration process was programmed to terminate if the discrepancy defined by formula (2.20) becomes less than specified value  $\delta = 10^{-5}$ . However, at  $R_s = 4.96$  the algorithm of critical point  $\zeta_c$  autodetection described in Section 2.2 failed to provide convergence of the Poisson equation solution due to the steady movement of critical point  $\zeta_c$  from the metal surface into the bulk. To obtain a definite result in this case, one had to turn off, after a number of initial iteration cycles,



the program module that redefined  $\zeta_c$ . Nevertheless, after such compulsory choice of critical point, the electron density jump in its vicinity did not drop lower than  $3 \cdot 10^{-4}$  in the course of iterations. At  $R_s > 5$  the convergence of iteration solution was not achieved at all. It appears that the crucial factor here, as concerns the algorithm operation, is that at  $R_s \rightarrow R_{sc}$  the effective potential (2.2) turns out almost equal to the local exchange-correlation one, and the contribution of the long-range Coulomb potential to forming the surface barrier becomes actually inessential.

The Table 1 demonstrates also the calculated  $R_s$  dependence of the work function  $W$ . In Fig. 7 this dependence (curve 3) is compared to similar ones presented in works [31] and [32]. The values of work function calculated in present work are in rather sensible agreement with

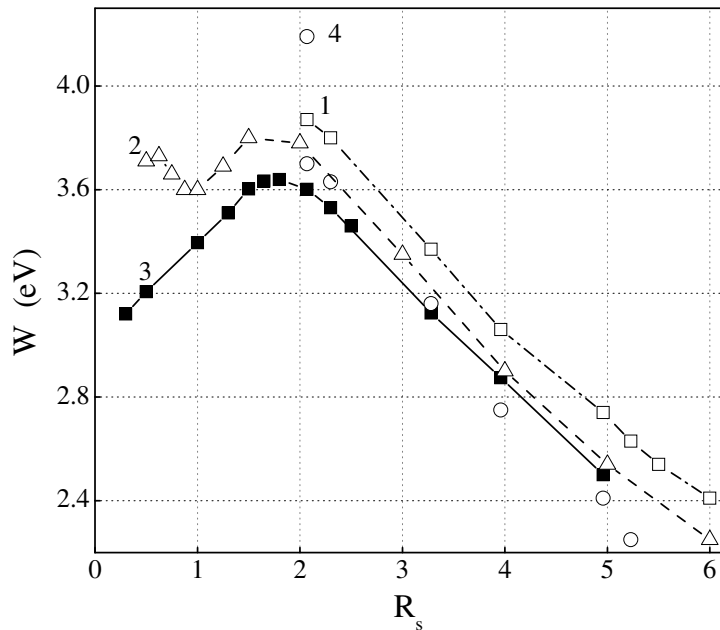


Figure 7: Work function in the homogeneous background model. Curves 1 and 2 represent results of calculations in [31] and [32]. Curve 3 was calculated in the present work. Circles 4 show experimental values of work function for polycrystalline specimens of Al, Li, Na, K and Rb from Table 3 of review [34]. The smaller of two  $W$  values at  $R_s = 2.07$  (Al) was measured in polycrystalline Al in the work [35].

experimental data for alkaline metals (Li ( $R_s = 3.28$ ), Na ( $R_s = 3.99$ ), K ( $R_s = 4.96$ )) and lie closer to measured values than those of curve 1 obtained in [31]. Most likely, the improved quantitative agreement between our calculations and experiment is a consequence of using the modified Wigner formula (2.9) for correlation energy, because at the same choice of expression for  $\varepsilon_c$  the results for the calculated potential are close to each other at least for  $R_s = 4$ , as can be seen in Fig. 6.

Our results for the work function at  $R_s > 1$  are in semi-quantitative agreement with those obtained in [32] (Fig. 7, curve 2), and this agreement improves with growing  $R_s$ . One can see from the figure that both curves have maxima at  $R_s \approx 2$ , however, at small  $R_s$  there is a qualitative difference. According to [32], work function has a local minimum at  $R_s \approx 1$ , which is not confirmed by our calculation. This local minimum in work function is possibly related to the absence of self-consistency in the solution of Kohn-Sham equations that has been obtained

in work [32] for small values of  $R_s$ .

The method of solution used in [32] and described in detail in work [36] replaces the Poisson equation with an integral equation for potential in some finite vicinity of metal surface and applies boundary conditions that do not fix the total charge (see. [36], Appendix A). Along with the problems noted in Section 1 in relation to the replacement of Poisson equation with integral one, such boundary conditions cannot provide a self-sustaining consistency of the final result of iteration procedure, as it was supposed in [32] (see the text after formula (7)). As mentioned in [32], the process failed to converge at all at  $R_s < 0.5$ . The reason for this lies probably in the increasing role of Coulomb potential compared to that of the exchange-correlation one and, therefore, the increasing sensitivity to self-consistency with a rise in electron density.

We note once more that the work [32] and ours are identical in the physical problem statement and in the formulation of initial equations except for different correlation energy formula used. At the same time, we faced no crucial difficulties with convergence at the region of small  $R_s$  and were limited only by growing requirements for computer memory and increased computation time caused by widening vacuum region with a non-zero electron density. As concerns the calculation problems in the region of large  $R_s$ , they require a further analysis and possibly relate in part to the use of local density approximation for the exchange-correlation potential. On the one hand, a ground for such premise can be found in the discussion on the application limits of local approximation for exchange-correlation interaction of electrons (see, for example, [37] and [38]). On the other hand, an attempt to apply directly an iteration procedure to the Kohn-Sham equation with potential  $U_{xc}$  in the absence of the Coulomb contribution to the effective potential has revealed that iterations failed to converge.

## 4.2 Surface energy

The self-consistent distributions of electron density and potential along with single-particle wave-functions obtained in our work allow to calculate the surface energy as a function of  $R_s$ . However, the formulae for calculating surface energy available in the literature use the finiteness of the region occupied by metal. On the one hand, this allows to find the surface energy as a difference between total energies of two states of the specimen before and after dividing it into two parts. On the other hand, this involves the quasidiscrete spectrum of eigenvalues and the necessity of precise evaluation of asymptotic dependence of total energy components on the specimen size as it tends to infinity (see, for example, [39]). To calculate the properties of an infinite specimen, one should have expressions for the densities of the corresponding components of total energy. In the standard formula of the density functional theory for the total energy of a finite specimen,

$$E_{\text{tot}}(N(\mathbf{r})) = T_s(N(\mathbf{r})) + \int d\mathbf{r} \varepsilon_{xc}[N(\mathbf{r})]N(\mathbf{r}) + \frac{1}{2} \int d\mathbf{r} d\mathbf{r}' \frac{(N(\mathbf{r}) - N_+)(N(\mathbf{r}') - N_+)}{|\mathbf{r} - \mathbf{r}'|}, \quad (4.4)$$

where integration is implied over the volume, the second and third terms describing the exchange-correlation and electrostatic energy of a many-electron system already include density definitions of the respective components. As concerns the total kinetic energy  $T_s$  of non-interacting electron gas, it does not possess such a property, being generally calculated by means of the formula obtained in [24] that expresses the sum of single-particle energies till the Fermi energy as the integral over the spectrum of the phase of continuous-spectrum wave functions with asymptotic form (2.35). Following the formula (50) in [1], we define the kinetic energy

density at zero temperature as

$$t_s(\mathbf{r}) = 2 \int_{\varepsilon \leq \varepsilon_F} \mathfrak{D} \{ \varepsilon \} \varepsilon |\Psi_\varepsilon(\mathbf{r})|^2 - U_{\text{eff}}(\mathbf{r})N(\mathbf{r}). \quad (4.5)$$

Using this expression, one can define the total energy density

$$\epsilon_{\text{tot}}(\mathbf{r}) = t_s(\mathbf{r}) + \varepsilon_{\text{xc}}[N(\mathbf{r})]N(\mathbf{r}) + \frac{1}{2}U(\mathbf{r})(N(\mathbf{r}) - N_+(\mathbf{r})) \quad (4.6)$$

and, accordingly, obtain the expression for the total energy in the volume  $V$  selected out of the infinite specimen,

$$E_{\text{tot}}(V) = \int_V d\mathbf{r} \epsilon_{\text{tot}}(\mathbf{r}), \quad (4.7)$$

which can be applied for calculating the surface energy.

The surface energy [3] in the jellium model becomes negative at  $R_s < 2.5$ , which means that metals with a high density of conduction electrons ( $2 < R_s < 2.5$ ) could not exist in such model. The surface energy values obtained in [3] differ the most drastically from the measured ones for multivalent metals, though even the case of monovalent metals of the first group demonstrates the increasing worsening of agreement between calculations and experiment with decreasing  $R_s$ . As it was shown, the main reason is that the jellium model neglects the discrete structure of the positive background, which is actually a crystal lattice of ion cores (see, for example, discussion in [34]). Nevertheless, it was interesting to find out if the use of self-consistent solution affects the  $R_s$  dependence of surface energy.

The surface energy was calculated using two expressions. One of them is based upon the strictly thermodynamical definition of surface energy as the component of total energy of a bulk homogeneous system, which depends on its surface area  $S$  rather than the volume  $V$ . Using, for instance, the definition (3.82) from [40], one can write

$$E_{\text{tot}} = S\Sigma + V\epsilon_{\text{tot}}, \quad (4.8)$$

where  $\Sigma$  is the surface energy density. In our case of semi-infinite specimen, the volume of the considered part of the system can be modified by receding from the surface to the bulk. Let us define the energy per unit area of the system region up to coordinate  $z$  by formula

$$E_{\text{tot}}(z) = \int_{-\infty}^z dz \epsilon_{\text{tot}}(z). \quad (4.9)$$

Since the energy density along with all variables defining it becomes constant in the bulk, the value of  $E_{\text{tot}}(z)$  should become a linear function of coordinate at sufficiently large  $z$ . Having continued this linear dependence back to the boundary of positive background, we obtain a finite value independent on the volume, which provides the surface energy by definition. The above can be expressed by simple formula

$$\Sigma = \lim_{z \rightarrow \infty} [E_{\text{tot}}(z) - \epsilon_{\text{tot}}(\infty)z]. \quad (4.10)$$

It is assumed here that the positive background boundary is at  $z = 0$ .

Such definition of surface energy is rigorous and, as a proper characteristic of a thermodynamical system, independent of the surface-forming process, which is sometimes modeled to determine the surface energy. However, it requires an enhanced accuracy in solving differential equations and calculating integrals, because the formula includes a difference of two large values. This difficulty is eliminated, if Eq. (4.10) is rewritten in the form

$$\Sigma = \int_{-\infty}^0 dz \epsilon_{\text{tot}}(z) + \int_0^{\infty} dz (\epsilon_{\text{tot}}(z) - \epsilon_{\text{tot}}(\infty)). \quad (4.11)$$

With such a formula for the surface energy, the result proves to be less sensitive to the accuracy of calculation, because the integrands tend to zero when receding from the surface.

In the literature, another definition of the surface energy is generally used, which represents it as a difference between the total energy of the semi-infinite specimen and that of a half of the infinite one (see, for example, [34]). Let us represent for convenience, as in work [3], the total surface energy density as a sum of kinetic, electrostatic and exchange-correlation components:

$$\Sigma = \Sigma_s + \Sigma_{\text{es}} + \Sigma_{\text{xc}} \quad (4.12)$$

In the dimensionless form and after integrating over the wave vector parallel to the surface in formula (4.5), the components of the surface energy density are written as

$$\begin{aligned} \sigma_s = \frac{1}{2\pi^2} \int_{-\infty}^{\infty} d\zeta \int_0^1 dk (1 - k^4) \left( |\psi_k(\zeta)|^2 - \frac{1}{2} \theta(\zeta) \right) - \\ - \frac{1}{3\pi^2} \int_{-\infty}^{\infty} d\zeta \{ (u(\zeta) + u_{\text{xc}}[n(\zeta)]) n(\zeta) - u_{\text{xc}}[1] \theta(\zeta) \} \end{aligned} \quad (4.13)$$

$$\sigma_{\text{xc}} = \frac{1}{3\pi^2} \int_{-\infty}^{\infty} d\zeta \{ \varepsilon_{\text{xc}}[n(\zeta)] n(\zeta) - \varepsilon_{\text{xc}}[1] \theta(\zeta) \} \quad (4.14)$$

$$\sigma_{\text{es}} = \frac{1}{6\pi^2} \int_{-\infty}^{\infty} d\zeta \{ n(\zeta) - 1 \cdot \theta(\zeta) \} u(\zeta). \quad (4.15)$$

The comparison of Eqs. (4.13)-(4.15) with the formulae (45a)-(45c) in work [34] reveals that only the expressions for the kinetic energy contribution  $\sigma_s$  are different. Using Eqs. (4.5) and (4.11) helped to avoid additional complications by eliminating integration of phase (2.37) of wave functions (2.35) over energy.

The results of surface energy calculation are presented in the Table 1. One can see that negative values of the surface energy appear at the values of  $R_s$ , even slightly larger than those reported in work [3]. The main reason for this is a smaller value of correlation energy given by formula (2.9). The general conclusion that the jellium model is insufficient to describe the surface energy in the domain of existence of real metals is still true.

## 5 Calculation of self-consistent potential of a Schottky barrier structure

Up to now, we considered the semi-infinite systems with purely real wave functions. As a consequence, such systems do not carry electric current. In this section, a structure is analyzed whose single-particle wave functions are limited and show oscillating behavior in both

infinitely far regions. Such boundary conditions for the Schrödinger equation solutions admit the complex eigenfunctions and system states with the nonzero stationary current. To avoid too laborious calculations in actually a model situation, we take a structure such as a metal-semiconductor contact with Schottky barrier. Because of a much larger free carrier density in the metal the potential barrier is almost totally formed in the semiconductor. This allows one to reduce the calculation part of the problem to finding the wave functions and the potential in a semi-infinite space and apply to this structure without any essential modification the iteration algorithm described in Section 2.2 for searching the self-consistent electron density and the effective potential barrier.

We restrict ourselves to the equilibrium situation when no bias voltage is applied to the structure and the current is zero. Let the metal occupy the region with  $z < 0$ , the degenerate n-type semiconductor with the ionized donor concentration  $N_D$  located at  $z > 0$ . For definiteness, we assume that high density of states at the metal-semiconductor boundary fixes the position of the conduction-band bottom at the interface at energy  $\Phi_s$  reckoned from the Fermi level. Since the under-barrier electron density in semiconductor near the interface is small, the effective potential coincides with the Coulomb one, thus defining the first boundary condition for electrostatic potential. The second boundary condition for solving the Poisson equation in the semiconductor region is specified by the requirement for the potential to be bounded at infinity, which means at the same time that the electric field turns to zero therein. Reckoning the energy from the value of potential in the bulk, we get the boundary conditions for solving the Poisson equation in the semiconductor,

$$U(0) \equiv U_0 = \Phi_s + \varepsilon_F, \quad \left. \frac{dU}{dz} \right|_{z=\infty} = 0 \quad (5.1)$$

Following the common practice, we neglect the penetration of electric field into the metal. Thus, the electrostatic potential in the metal is assumed to be constant and equal to its value at the interface.

To describe the single-particle states of continuous spectrum in such one-dimensional inhomogeneous structure, we use the results of the analysis carried out in [2] of the Hilbert space related to the Hamiltonian of infinite system. We take as a basis the wave functions of the right-hand  $\Psi^R$  and the left-hand  $\Psi^L$  states

$$\Psi_{k,\mathbf{k}_{\parallel}}^R(z, \mathbf{r}_{\parallel}) = C_k^R \psi_k^R(z) \exp(i\mathbf{k}_{\parallel} \mathbf{r}_{\parallel}) / 2\pi, \quad (5.2)$$

$$\Psi_{q,\mathbf{k}_{\parallel}}^L(z, \mathbf{r}_{\parallel}) = C_q^L \psi_q^L(z) \exp(i\mathbf{k}_{\parallel} \mathbf{r}_{\parallel}) / 2\pi, \quad (5.3)$$

which are uniquely defined by their asymptotic behavior at infinity,

$$\psi_k^R(z) = \begin{cases} e^{-ikz} + r_k^R e^{ikz} & z \rightarrow \infty \\ t_k^R e^{-iqz} & z \rightarrow -\infty \end{cases} \quad (5.4)$$

and

$$\psi_q^L(z) = \begin{cases} e^{iqz} + r_q^L e^{-iqz} & z \rightarrow -\infty \\ t_q^L e^{ikz} & z \rightarrow \infty \end{cases} \quad (5.5)$$

Using two quantum numbers  $k$  and  $q$  to describe the asymptotic behavior of eigenfunctions in the right-hand and left-hand infinite regions is related to the asymmetry of the considered barrier structure even in the absence of bias voltage. This asymmetry is caused by different positions of conduction-band bottom in the metal and in the semiconductor with respect to

the Fermi level. Besides, even a symmetric structure becomes asymmetric when biased, so the different quantum numbers are rather a rule than an exception. The relation between  $k$  and  $q$  is found from the condition that both characterize the eigenfunction pertaining to the same eigenvalue  $\varepsilon$  of the Hamiltonian,

$$\varepsilon - U_{xc}(\infty) = \frac{q^2 + \mathbf{k}_{\parallel}^2}{2m_M} + U_M = \frac{k^2 + \mathbf{k}_{\parallel}^2}{2m_S}, \quad (5.6)$$

Here  $U_M$  is the position of conduction-band bottom in the metal reckoned from that in the semiconductor, and indices M and S denote the effective masses in metal and in semiconductor, respectively. The right-hand equality in Eq. (5.6) defines  $q$  as an implicit function of  $k$  (and vice versa). Normalization constants  $C_q^L$  and  $C_k^R$  equal  $1/\sqrt{2\pi}$  if  $\psi_q^L$  are normalized to  $\delta(q - q')$  and  $\psi_k^R$  are normalized to  $\delta(k - k')$ . The proof of mutual orthogonality of the pair of functions  $\Psi_{\varepsilon}^{R,L}$  at one energy value  $\varepsilon$ , which is necessary to have a full orthonormalized basis in the Hilbert space of the problem, was presented in [2].

However, in the considered structure, all the results can be expressed in values related to the semiconductor electrode of the metal-semiconductor contact, so it is more convenient to normalize  $\psi_q^L$  also to  $\delta(k - k')$ . In this case, for the normalization constant of the left-hand states one should use the expression

$$|C_k^L|^2 = \frac{1}{2\pi} \frac{\partial q}{\partial k}. \quad (5.7)$$

Solving the problems where the self-consistency is unnecessary, one usually normalizes the wave functions of continuous spectrum to the unit amplitude of incident wave. It is sufficient to calculate the tunneling transparency for the barrier of specified shape. However, to find the self-consistent solution taking into account the Coulomb interaction of charge carriers one has to know the spatial distribution of electrons, which is impossible without calculating the continuous-spectrum eigenfunctions normalized to the delta-function of quantum numbers.

Let us adduce the relations between the reflectivity  $r$  and the transparency  $t$  of the barrier, which are necessary to carry out the calculations:

$$\frac{1}{\partial q / \partial k} |t_k^R|^2 = 1 - |r_k^R|^2, \quad \frac{1}{\partial k / \partial q} |t_q^L|^2 = 1 - |r_q^L|^2. \quad (5.8)$$

$$t_{q(k)}^L = \frac{1}{\partial q / \partial k} t_k^R, \quad r_{q(k)}^L = -r_k^{R*} (t_k^R / t_k^{R*}). \quad (5.9)$$

Eqs. (5.9) are written for the case of left-hand states normalized to  $\delta(k - k')$ , which is indicated by explicit dependence  $q(k)$  in the arguments.

The electron wave function in semiconductor can be represented as a superposition of two real linearly independent solutions  $\phi_1$  and  $\phi_2$ , which at  $z \rightarrow \infty$  have the following asymptotic behavior:

$$\begin{aligned} \phi_{k1}(z) &= \sin(kz + \gamma_k), \\ \phi_{k2}(z) &= \cos(kz + \gamma_k), \end{aligned} \quad (5.10)$$

where  $\gamma_k$  is the phase of the wave function of  $k$ -th state. With these functions, using boundary conditions and normalization, one can build  $\psi_k^R(z)$ , which, in its turn, is sufficient to define  $\psi_q^L(z)$ .

The solutions  $\phi_1$  and  $\phi_2$  are found by means of integration of the Cauchy problem for the Schrödinger equation (2.34). With argument  $z$  receding from the interface into the bulk,

functions  $\phi_1$  increase exponentially in the under-barrier region while  $\phi_2$  decrease. If the potential barrier is high enough, searching for the exponentially vanishing solution presents some calculation difficulties. To overcome them, the following technique was employed. Function  $\phi_1$  is found from the Cauchy problem solution with the initial conditions  $\phi_{k1}(0) = 1$  and  $\phi'_{k1}(0) = \sqrt{U_0 - k^2/2}$  specified at the metal-semiconductor interface  $z = 0$ . Eq. (2.34) is integrated from  $z = 0$  to  $z_\infty$  into the semiconductor bulk where the effective potential becomes constant to a sufficient degree of accuracy. The solution obtained is normalized to the unit amplitude by formula similar to Eq. (2.36), and phase  $\gamma$  in expressions (5.10) is found with the help of relation (2.37). It should be noted that choice of initial conditions for  $\phi_1$  is quite arbitrary, because the normalization procedure provides the correct asymptotic behavior of solutions at infinity. To find  $\phi_2$ , one also solves the Cauchy problem, but the initial conditions are imposed this time at the point  $z = z_\infty$ :

$$\begin{aligned}\phi_{k2}(z_\infty) &= \cos(kz_\infty + \gamma_k) \\ \phi'_{k2}(z_\infty) &= -k\phi_{k1}(z_\infty)\end{aligned}\tag{5.11}$$

and the integration is carried out from the semiconductor bulk to metal boundary in the direction of the  $\phi_{k2}(z)$  growth in the barrier region thus improving the stability of procedure. The accuracy criterion for the pair of solutions obtained is the constancy of the Wronskian  $W(\phi_{k1}, \phi_{k2})$  at the interval  $[0, z_\infty]$ .

Further on we assume that the effective masses of electrons in semiconductor and metal are equal. Then both the wave function itself and its first derivative are continuous at the boundary of the two media. Of course, such premise is rather simulative, but the complicated problem of deriving the matching conditions for the envelope wave functions at the metal-semiconductor interface is not the subject of our work. A different type of boundary condition at the interface may, of course, affect the particular numerical results, but this will hardly require a change in the iteration scheme suggested for solving the Kohn-Sham equations for the structures with the current states. The reasons for such opinion will be discussed at the end of this section. Note also that problems close to those considered here arise as well in the theory of resonant tunneling diodes (see, for example, [41]).

## 5.1 Some calculation details

Now then, on the basis of two functions (5.10) we should form the wave function  $\psi_k^R(z)$  of the "right-hand" state that describes the tunneling of electrons from the right-hand (semiconductor) electrode into the left-hand one, which we still call for convenience "the metal". The asymptotic boundary conditions (5.4) defining  $\psi_k^R(z)$  realize the requirement to have a purely outgoing wave in the metal and a linear combination of incident and reflected waves in the semiconductor. These conditions can be used to find the coefficients in the expansion

$$\psi_k^R(z) = \alpha_k \phi_{k1}(z) + \beta_k \phi_{k2}(z).\tag{5.12}$$

When  $\psi_k^R$  is found,  $\psi_k^L$  in general form can be represented as a linear combination of two independent solutions  $\psi_k^R$  and  $\psi_k^{R*}$ . But to calculate the electron density in the semiconductor, which is what we only need for the problem to be solved, one has to know  $\psi_k^L(z)$  only at  $z \geq 0$ . So to express  $\psi_k^L$  through  $\phi_{k1,2}$  it is enough to take advantage of the asymptotic form (5.10) of the left-hand state at  $z \rightarrow \infty$ . All the above considering, one easily obtains

$$\psi_{q(k)}^L(z) = t_{q(k)}^L \exp(-i\gamma_k)(i\phi_{k1}(z) + \phi_{k2}(z)).\tag{5.13}$$

The problem of defining  $\psi_k^R(z)$  reduces to finding four complex coefficients  $\alpha_k, \beta_k, r_k^R, t_k^R$ . The four corresponding equations are obtained by equating the asymptotic formulae for function  $\psi_k^R$  and its derivative at  $z \rightarrow \infty$  to the asymptotic form of the linear combination required, which provides two equations, and also from two matching conditions for the function and its derivative at the boundary  $z = 0$ . In so doing, we assume that in the metal

$$\psi_k^R(kz) = t_k^R \exp(-iq(k)z). \quad (5.14)$$

The calculation is carried out under the condition  $U_M < 0$ , which provides that the conduction band bottom in the left-hand electrode is lower than that in the right-hand one, so that inequality  $q(\varepsilon, \mathbf{k}_{\parallel}) \neq k(\varepsilon, \mathbf{k}_{\parallel})$  remains valid in spite of the assumed equality of effective masses in the electrodes. At the same time, the condition of effective mass equality ensures that function  $q(k)$  is independent of  $\mathbf{k}_{\parallel}$ , which reduces the computational cost.

With some simple transformations, the sought system of linear algebraic equations takes the form

$$\begin{aligned} \alpha\phi_{k1}(0) + \beta\phi_{k2}(0) - t_k &= 0, \\ \alpha\phi'_{k1}(0) + \beta\phi'_{k2}(0) + iqt_k &= 0, \\ i\alpha + \beta &= 2\exp(i\gamma_k), \\ i\alpha - \beta + 2r_k \exp(-i\gamma_k) &= 0. \end{aligned} \quad (5.15)$$

For brevity, we omit everywhere the index R of the right-hand state, the wave-number index  $k$  of coefficients  $\alpha, \beta$ , and imply that  $q = q(k)$ .

The solution of system (5.15) can be represented as

$$r_k = -\frac{(q\Phi_k + i\Phi'_k)^*}{q\Phi_k + i\Phi'_k}, \quad (5.16)$$

$$t_k = \Phi_k^* + r_k\Phi_k, \quad (5.17)$$

$$\alpha_k = -i(\exp(i\gamma_k) - r_k \exp(-i\gamma_k)), \quad (5.18)$$

$$\beta_k = \exp(i\gamma_k) + r_k \exp(-i\gamma_k), \quad (5.19)$$

where for compactness we introduced functions

$$\Phi_k = \exp(-i\gamma_k) (\phi_{k2}(0) + i\phi_{k1}(0)), \quad (5.20)$$

$$\Phi'_k = \exp(-i\gamma_k) (\phi'_{k2}(0) + i\phi'_{k1}(0)), \quad (5.21)$$

and  $\phi'_k$  means the derivative by  $z$ .

The scheme presented for calculating wave functions describes a modified procedure for solving the Schrödinger equation (2.17) for unbounded system as distinct from a semi-bounded one (see Section 2.2). The corresponding formula to replace Eq. (2.38) for calculating the electron density in a barrier structure is found from the general expression derived in [2]. Taking into account that the electron density should be known only at  $z \geq 0$ , and the absence of bias voltage, we get

$$N(z) = 2 \int_0^\infty dk \int_{-\infty}^\infty d\mathbf{k}_{\parallel} f(\varepsilon(k, \mathbf{k}_{\parallel})) \left[ |\Psi_{q(k)}^L(z)|^2 + |\Psi_k^R(z)|^2 \right], \quad (5.22)$$

where  $f(\varepsilon)$  is the Fermi distribution function, and energy eigenvalues  $\varepsilon(k, \mathbf{k}_{\parallel})$  are given by formula (5.6). The Fermi level position is defined by the neutrality condition in the semiconductor



bulk at  $z \rightarrow \infty$ . Using the definitions (5.2)-(5.3), (5.7), and (5.12)-(5.13) along with relations (5.8)-(5.9) between the amplitude coefficients of barrier reflection and transparency, we obtain from (5.22) an expression for electron density in terms of the two real solutions  $\phi_{k1,2}(z)$  found numerically,

$$N(z) = \frac{2}{(2\pi)^3} \int_0^\infty dk \int_{-\infty}^\infty d\mathbf{k}_\parallel f(\varepsilon(k, \mathbf{k}_\parallel)) \times \left[ |\alpha_k \phi_{k1}(z) + \beta_k \phi_{k2}(z)|^2 + \left(1 - |r_k^R|^2\right) |\phi_{k1}(z) - i\phi_{k2}(z)|^2 \right]. \quad (5.23)$$

Here the coefficients  $r_k^R$ ,  $\alpha_k$ , and  $\beta_k$  are defined in (5.16)-(5.19).

The expression (5.23) for electron density provides an explicit representation of the formula (2.18) of iteration procedure for the case under consideration.

## 5.2 Results and discussion

Calculations were carried out at the values of parameters typical for the Al/n-GaAs junctions ( $m^* = 0.07m_e$ ,  $\Phi_s = 0.9$  eV,  $\kappa = 12.5$ ) with ionized donor concentration  $N_D = 10^{18} \text{cm}^{-3}$ , which corresponds to  $R_s = 0.66$ . For  $q$ , in virtue of the large difference between Fermi energies in semiconductor and aluminium, it turned out possible to accept a constant value that was chosen equal to the radius of the Fermi surface of electron gas at  $R_s = 2.07$ ,  $\kappa_m = 1$ . Fig. 8

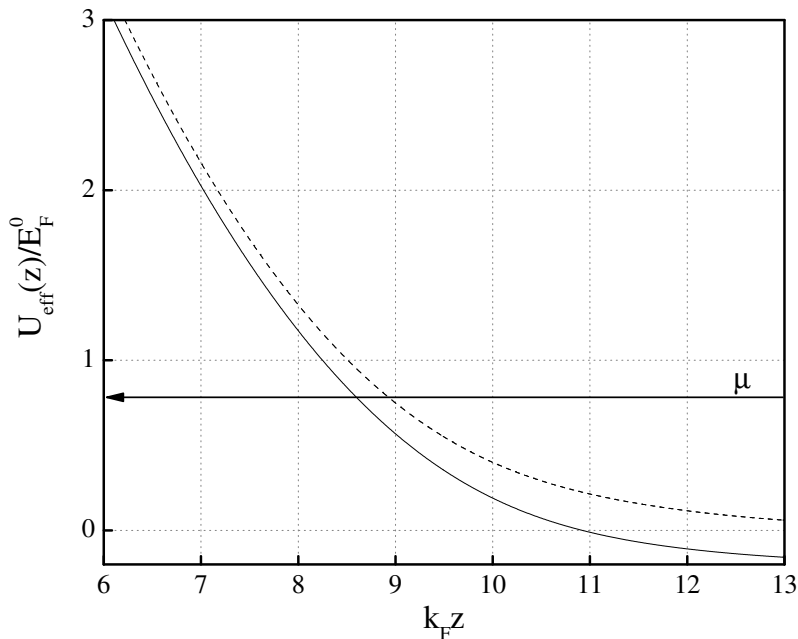


Figure 8: Self-consistent potential for a Schottky barrier structure ( $R_s = 0.66$ ). Solid line represents the potential found with account of exchange-correlation interaction, dashed line is the potential in Hartree approximation. The Fermi level position with account of  $U_{xc}$  is marked.

represents the coordinate dependence of the self-consistent effective potential calculated with account of the exchange-correlation potential of the electrons (curve 1) and in Hartree approximation (curve 2) near the metal-semiconductor interface. One can see that including  $U_{xc}$  into

calculation modifies the potential barrier shape making the drop of potential steeper. This difference has a notable impact on the shape of theoretical current-voltage curve of tunneling junction, particularly in the case of forward bias when electrons tunnel from semiconductor into metal through the effective potential barrier region below the Fermi level (see [10], [42]-[43]). It is demonstrated in the same works that the account of  $U_{xc}$  allows describing more accurately the current-voltage curves of real structures. Hence, the representation of the exchange-correlation interaction of electrons by means of the local density approximation remains quite accurate for the electron states located sufficiently deep under the Fermi level.

Besides, the use of self-consistent solution for potential in the tunneling current formula makes possible to define the parameters  $\Phi_s$  and  $N_D$  of the metal/heavily n-doped GaAs junction from the bias voltage dependence of differential resistance [44]-[46]<sup>1</sup>. The Schottky barrier was calculated there in the Thomas-Fermi and Thomas-Fermi-Gombas approximations. Though in such structures the conditions are well fulfilled for the Schottky barrier to be quasiclassical, i. e.  $k_F L \gg 1$  and  $k_F l_{TF} \gg 1$ , where  $L$  and  $l_{TF}$  denote the characteristic scales of spatial variations of the self-consistent potential inside and outside the barrier [44], the question of a possible notable change in barrier shape beyond the scope of the Thomas-Fermi approximation still remained. The exact calculation showed that the large-scale behavior of the Schottky-barrier effective potential is accurately described by the potential found in the Thomas-Fermi approximation, and the agreement between them improves with decreasing  $R_s$ .

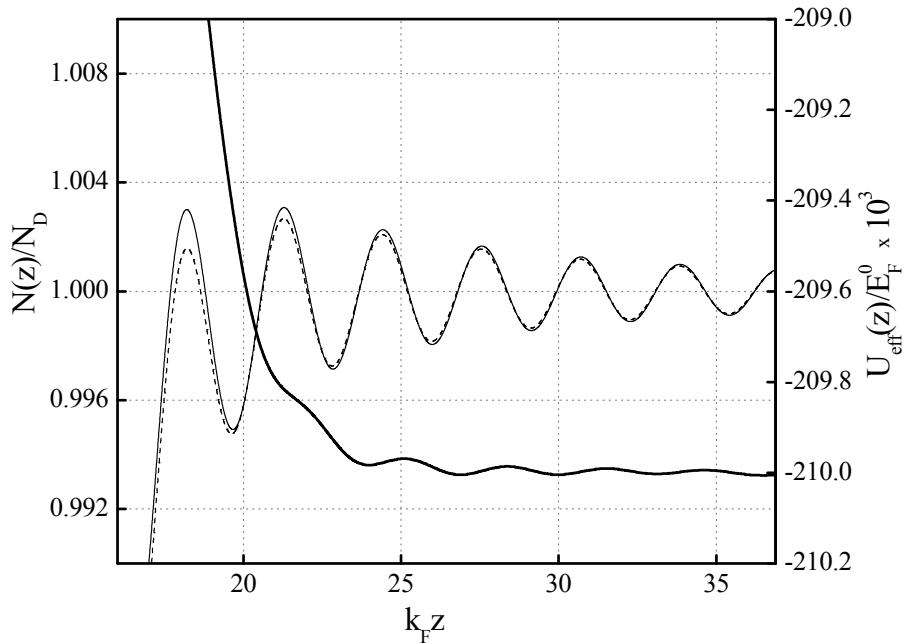


Figure 9: Friedel oscillations of electron density and effective potential in the Schottky barrier structure at  $R_s = 0.66$ . Solid line is electron density with account of exchange-correlation interaction, dashed line is electron density in the Hartree approximation. Bold solid line is the self-consistent effective potential.

In the semiconductor bulk, the coordinate dependence of self-consistent potential and electron density manifests oscillations (Fig. 9), which are absent in the Thomas-Fermi approximation. As a whole, the oscillations caused by Schottky barrier are less pronounced than those in

<sup>1</sup>The Fig.3 missed in the published version of the Ref. [46] is restored in the arXiv preprint.

the case of an infinitely high potential wall (compare with Fig. 4), which is apparently related to the quasiclassical smoothness of the Schottky barrier. This is particularly true in regard to the effective potential oscillations. As can be seen in Fig. 9, the oscillation magnitude of effective potential is quite small, of the order of  $10^{-4}$  and less, while the electron density oscillations in the exact solution are, on the contrary, more intensive than those in the Hartree approximation. The suppression of the effective potential oscillations compared to those of its Coulomb component was already discussed in Section 3.1. The amplification of density oscillations in the exact solution with respect to solution in the Hartree approximation can be explained by analyzing the linearized expression for the induced density.

It is well known that linearization of formula (2.7) in the Hartree approximation at small values of potential  $U$  leads in the self-consistent Poisson equation (2.12) to the expression for the density (charge) increment, which is generally written as  $4\pi\delta N_{\text{ind}} = -k_{\text{TF}}^2 U$ . The account of the electron density dependence of exchange-correlation potential leads to a similar relation  $4\pi\delta N_{\text{ind}} = -k_{\text{scr}}^2 U$ , the inverse square screening length being

$$k_{\text{scr}}^2 = \frac{k_{\text{TF}}^2}{1 + \frac{3}{2} du_{\text{xc}}(n)/dn}. \quad (5.24)$$

The dimensionless exchange-correlation potential grows in absolute magnitude with decreasing electron concentration, so the derivative  $du_{\text{xc}}/dn < 0$ , and the denominator in formula (5.24) tends to zero with growing  $R_s$ . The equality of the denominator to zero provides the critical value of  $R_{\text{sc}}$ . So, at comparable values of the self-consistent potential oscillations in the exact solution and that obtained in the Hartree approximation, which is in evidence, the electron density oscillations in the exact solution will be amplified increasingly with  $R_s$  getting closer to  $R_{\text{sc}}$ . Accordingly, the screening region, where the perturbation drops exponentially, will be reduced.

Summarizing the results of analyzing the Friedel-type oscillations caused by the violation of homogeneity of degenerate electron gas, we note that the account of exchange-correlation interaction of electrons leads to the increase of electron density oscillations and the decrease of effective-potential oscillations with respect to results obtained in the Hartree approximation.

To conclude this section, let us discuss to what extent the results obtained depend on the adopted condition of equal effective masses in the two electrodes. Generally speaking, the problem of boundary conditions for the envelope function at the interface of two solids differing not only by effective masses, but also by the type of charge carriers and their dispersion law, is rather complicated. According to the current opinion, such conditions cannot be reduced to a universal relation between the values of wave function and its derivative on both sides of the interface, but should be derived for each specific case (see, for example, the critical discussion related to heterojunctions in [47], [48]).

Staying within the framework of phenomenological description of boundary conditions, one can write them in the most general form in terms of the transfer matrix  $\mathbb{T}$ , the elements of which are constrained by the requirement of Hermiticity of the Hamiltonian [48]. If envelope-function equations for both electrodes can be taken in the single-band approximation, the boundary conditions are described by a  $2 \times 2$  matrix. In the case when the  $\mathbb{T}$ -matrix can be diagonal [49], the final formulae (5.16)-(5.19) keep their form with the barrier transparency  $t_k$  and wave vector  $q$  replaced by renormalized values  $\tilde{t} = T_{11}t_k$  and  $\tilde{q} = (T_{22}/T_{11})q$ .

If matrix  $\mathbb{T}$  has the nonzero off-diagonal elements, it does not lead to crucial difficulties in building the R- and L-solutions of the Schrödinger equation according to their asymptotic behavior at  $z \rightarrow \pm\infty$  from the particular real solutions. However, the analysis of the most

general case in this work would make the statement of fundamental aspects of iteration algorithm application unreasonably cumbersome. At the same time, the inequality of wave vectors  $q(\varepsilon) \neq k(\varepsilon)$  typical for the non-symmetrical barrier structures was necessary to include into the calculation.

## 6 Conclusion

The realized iteration algorithm for solving the self-consistent field equations was found to converge in all the cases considered of typical inhomogeneous electron systems with continuous spectrum. The difficulties of its application arose only when considering the jellium model at large values of  $R_s \geq 5$  that do not occur in most metals and semiconductor structures. It was also shown that an explicit account of screening properties of electron gas in the algorithm for numerical analysis of infinite Coulomb systems allows to consider a selected limited volume of such system, transferring the boundary conditions from infinity to the surface and assuming the energy spectrum of single-electron states to be strictly continuous. Such approach also eliminates the difficulties that arise when considering an inhomogeneous infinite system with continuous spectrum as a limit of a finite one with quasi-discrete spectrum.

This work was partially supported by Russian Foundation for Basic Research with grants 07-02-01481 and 06-02-16955.

## References

- [1] W. Kohn and P. Vashishta, In *Theory of the inhomogeneous electron gas*, ed. by S. Lundqvist and N.H. March, Plenum Press, N-Y. (1983), Ch. 2
- [2] A.Ya. Shul'man, J. Phys.: Conf. Ser. **35**, 163 (2006)
- [3] N. D. Lang and W. Kohn, Phys. Rev. B **1**, 4555 (1970)
- [4] M. Manninen, R. Nieminen, P. Hautojarvi, J. Arponen, Phys. Rev. B **12**, 4012 (1975)
- [5] A. Liebsch, *Electronic Excitations at Metal Surfaces*, Plenum Press, New York (1997), Sec. 2.3.2
- [6] R.M. Nieminen, J. Phys. F, **7**, 375 (1977)
- [7] A.Ya. Shul'man, D.V. Posvyanskii, arXiv: cond-mat/0209335
- [8] D. Pines, *Elementary Excitations in Solids*, Benjamin, N-Y, 1963
- [9] P. Gombás, *Theorie des Atoms und Ihre Anwendungen*, Springer Verlag, Wien (1949)
- [10] A.Ya. Shul'man, V.V. Zaitsev, Sol. State Comm., **18**, 1623 (1976)
- [11] S.K. Godunov, V.S. Ryaben'kii, *Difference schemes*, Nauka, Moscow (1977) (in russian)
- [12] O.V. Konstantinov, A.Ya. Shik, ZhETF, **58**, 1662 (1970)
- [13] J.F. Appelbaum and G.A. Baraff, Phys. Rev. Lett **26**, 1432 (1971)
- [14] R.G. Newton, *Scattering Theory of Waves and Particles*, McGraw-Hill, New York, 1966
- [15] G.A. Baraff and J.F. Appelbaum, Phys. Rev. B **5**, 475 (1972)
- [16] R.P. Fedorenko, *Introduction in Computational Physics*, Izd. MFTI, Moscow (1994), §15 (in russian)
- [17] T. Ando, A.B. Fowler, F. Stern, Rev. Mod. Phys. **54**, 437 (1982)
- [18] J. Suñé, P. Olivo, B. Riccó, J. Appl. Phys. **70**, 337 (1991)
- [19] C.A. Mead, Phys. Rev. Lett. **6**, 545 (1961)
- [20] M. Stengel and N.A. Spaldin, Nature **443**, 679 (2006)
- [21] H.Y. Ku and F.G. Ullman, J. Appl. Phys. **35**, 265 (1964)
- [22] C.T. Black and J.J. Welser, IEEE Trans. **ED 46**, 776 (1999)
- [23] J. Bardeen, Phys. Rev. **49**, 653 (1936)
- [24] H.B. Huntington, Phys. Rev. **81**, 1035 (1951)
- [25] L.J. Sinnamon, R.M. Bowman J.M. Gregg, Appl. Phys. Lett. **78**, 1724 (2001)

- [26] H. Ehrenreich and H.R. Philipp, Phys. Rev. **128**, 1622 (1962)
- [27] W.S. Choi, S.S.A. Seo, K.W. Kim et al, Phys. Rev. **B 74**, 205117 (2006)
- [28] K.M. Rabe, Nature Nanotechnology **1**, 171 (2006)
- [29] W. Kohn and C. Majumdar, Phys. Rev. **138**, A1617 (1965)
- [30] D. C. Tsui, Phys. Rev. B **8**, 2657 (1973)
- [31] N.D. Lang and W.Kohn, Phys. Rev. B **3**, 1251 (1971)
- [32] J.P. Perdew and Y. Wang, Phys. Rev. B **38**, 12228 (1988)
- [33] H.F. Budd and J. Vannimenus, Phys. Rev. Lett. **31**, 1281, 1430 (Erratum) (1973)
- [34] N.D. Lang, In *Theory of the inhomogeneous electron gas*, ed. by S. Lundqvist and N. H. March, Plenum Press, N-Y. (1983), Ch. 5
- [35] B. Sieroszynska-Wojas, FTT **10**, 693 (1968)
- [36] R. Monnier and J. P. Perdew, Phys. Rev. B **17**, 2595 (1978)
- [37] R. O. Jones and O. Gunnarsson, Rev. Mod. Phys. **61**, 689 (1989)
- [38] W. Kohn, Rev. Mod. Phys., **71**, 1253 (1999)
- [39] G. Paasch and M. Hietschold, *Die Oberfläche der festen Körper. In: Ergebnisse in der Elektronentheorie der Metalle*, eds P. Ziesche and G. Lehmann, Akademie-Verlag, Berlin (1983), Ch. 10
- [40] M.A. Leontovich, *Introduction in Thermodynamics*, Nauka, Moscow (1983), Ch. 3 (in russian)
- [41] D. K. Ferry and S. M. Goodnick *Transport in Nanostructures*, Cambridge Uni Press, Cambridge, UK (1997)
- [42] I.N. Kotel'nikov, A.Ya. Shul'man, *Proc. 19th Int. Conf. on Phys. Semicond.*, Warsaw (1988), Vol. 1, p. 681
- [43] A.Ya. Shul'man, I.N. Kotel'nikov, N.A. Varvanin et al, Pis'ma v ZhETF, **73**, 643 (2001)
- [44] I.N. Kotel'nikov, I.L. Beinikhes, A.Ya. Shul'man, FTT **27**, 401 (1985)
- [45] I.N. Kotel'nikov, D.K. Chepikov, E.G. Chirkova et al, FTP **21**, 1854 (1987)
- [46] E.M.Dizhur, A.Ya. Shul'man, I.N. Kotel'nikov, A.N.Voronovsky, phys. stat. sol. (b) **223**, 129 (2001); arXiv:cond-mat/0010200
- [47] E.E. Takhtamirov, V.A. Volkov, ZhETF **116**, 1843 (1999).
- [48] I.V. Tokatly, A.G. Tsibizov, A.A. Gorbatsevich, Phys. Rev. B **65**, 165328 (2002)
- [49] T. Ando, S. Wakahara, H. Akera, Phys. Rev. B **40**, 11609 (1989)